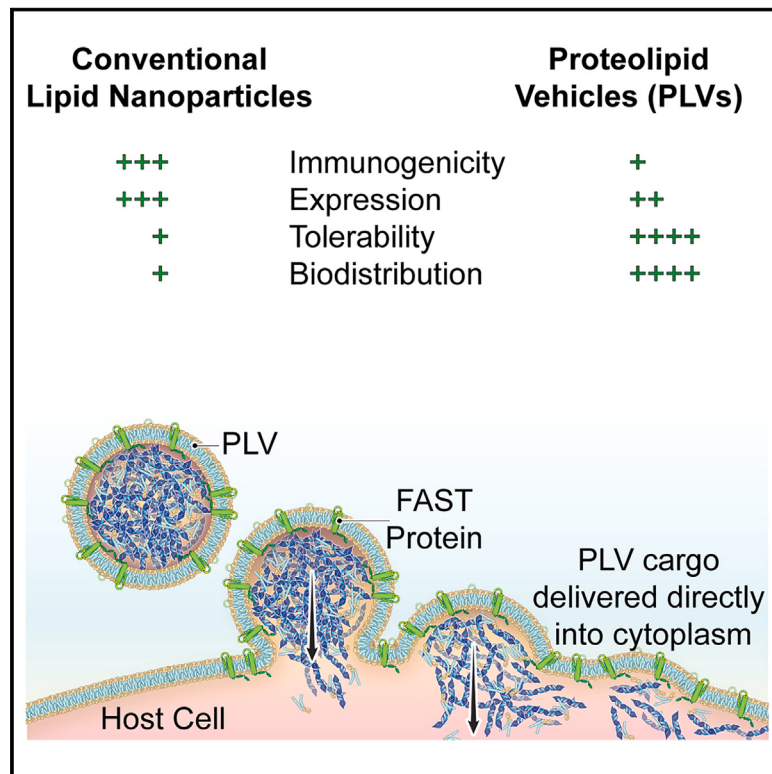


# Safe and effective *in vivo* delivery of DNA and RNA using proteolipid vehicles

## Graphical abstract



## Authors

Douglas W. Brown, Ping Wee,  
Prakash Bhandari, ..., Roy Duncan,  
Arun Raturi, John D. Lewis

## Correspondence

arun.raturi@entospharma.com (A.R.),  
jidlewis@ualberta.ca (J.D.L.)

## In brief

Current genetic medicines are limited by tolerability, scalability, and immunogenicity issues. Utilizing components from viral and non-viral delivery platforms, we developed a lipid-based delivery vehicle formulated with a chimeric fusion protein that delivers nucleic acid cargo inside cells effectively and with broad distribution and low immunogenicity. This proteolipid vehicle platform is suitable for safe and effective repeat dosing of DNA and/or RNA *in vivo*.

## Highlights

- Adding FAST protein to a lipid formulation increases mRNA and pDNA expression
- FAST-PLVs show high degrees of extrahepatic gene delivery with mRNA and pDNA
- The low immunogenicity of the FAST-PLV platform enables repeat dosing
- Systemically administered FAST-PLVs facilitate therapeutic pDNA gene expression

Article

# Safe and effective *in vivo* delivery of DNA and RNA using proteolipid vehicles

Douglas W. Brown,<sup>1,2</sup> Ping Wee,<sup>2</sup> Prakash Bhandari,<sup>2</sup> Amiralı Bukhari,<sup>1,2</sup> Liliya Grin,<sup>2</sup> Hector Vega,<sup>2</sup> Maryam Hejazi,<sup>1,2</sup> Deborah Sosnowski,<sup>1</sup> Jailal Ablack,<sup>2,3</sup> Eileen K. Clancy,<sup>4</sup> Desmond Pink,<sup>1</sup> Jitendra Kumar,<sup>2</sup> Maria Paola Solis Ares,<sup>2</sup> Suellen Lamb,<sup>1,2</sup> Rodrigo Quevedo,<sup>2</sup> Bijal Rawal,<sup>2</sup> Fahed Elian,<sup>2</sup> Natasha Rana,<sup>2</sup> Luis Morales,<sup>2</sup> Natasha Govindasamy,<sup>2</sup> Brendan Todd,<sup>2</sup> Angela Delmage,<sup>2</sup> Somnath Gupta,<sup>2</sup> Nichole McMullen,<sup>4</sup> Duncan MacKenzie,<sup>4</sup> Perrin H. Beatty,<sup>2</sup> Henry Garcia,<sup>5</sup> Manoj Parmar,<sup>2</sup> Jennifer Gyoba,<sup>2</sup> Chandra McAllister,<sup>2</sup> Matthew Scholz,<sup>5</sup> Roy Duncan,<sup>2,4</sup> Arun Raturi,<sup>1,2,\*</sup> and John D. Lewis<sup>1,2,3,5,6,\*</sup>

<sup>1</sup>Department of Oncology, University of Alberta, Edmonton, AB T6G 2E1, Canada

<sup>2</sup>Entos Pharmaceuticals, 10230 Jasper Avenue, Suite 4550, Edmonton, AB T5J 4P6, Canada

<sup>3</sup>OncosensX, 701 Fifth Avenue, Suite 4200, Seattle, WA 98104, USA

<sup>4</sup>Department of Microbiology & Immunology, Dalhousie University, Halifax, NS B3H 4R2, Canada

<sup>5</sup>Oisin Biotechnologies, 701 Fifth Avenue, Suite 4200, Seattle, WA 98104, USA

<sup>6</sup>Lead contact

\*Correspondence: [arun.raturi@entospharma.com](mailto:arun.raturi@entospharma.com) (A.R.), [jdlLewis@ualberta.ca](mailto:jdlLewis@ualberta.ca) (J.D.L.)

<https://doi.org/10.1016/j.cell.2024.07.023>

## SUMMARY

Genetic medicines show promise for treating various diseases, yet clinical success has been limited by tolerability, scalability, and immunogenicity issues of current delivery platforms. To overcome these, we developed a proteolipid vehicle (PLV) by combining features from viral and non-viral approaches. PLVs incorporate fusion-associated small transmembrane (FAST) proteins isolated from fusogenic orthoreoviruses into a well-tolerated lipid formulation, using scalable microfluidic mixing. Screening a FAST protein library, we identified a chimeric FAST protein with enhanced membrane fusion activity that improved gene expression from an optimized lipid formulation. Systemically administered FAST-PLVs showed broad biodistribution and effective mRNA and DNA delivery in mouse and non-human primate models. FAST-PLVs show low immunogenicity and maintain activity upon repeat dosing. Systemic administration of follistatin DNA gene therapy with FAST-PLVs raised circulating follistatin levels and significantly increased muscle mass and grip strength. These results demonstrate the promising potential of FAST-PLVs for redosable gene therapies and genetic medicines.

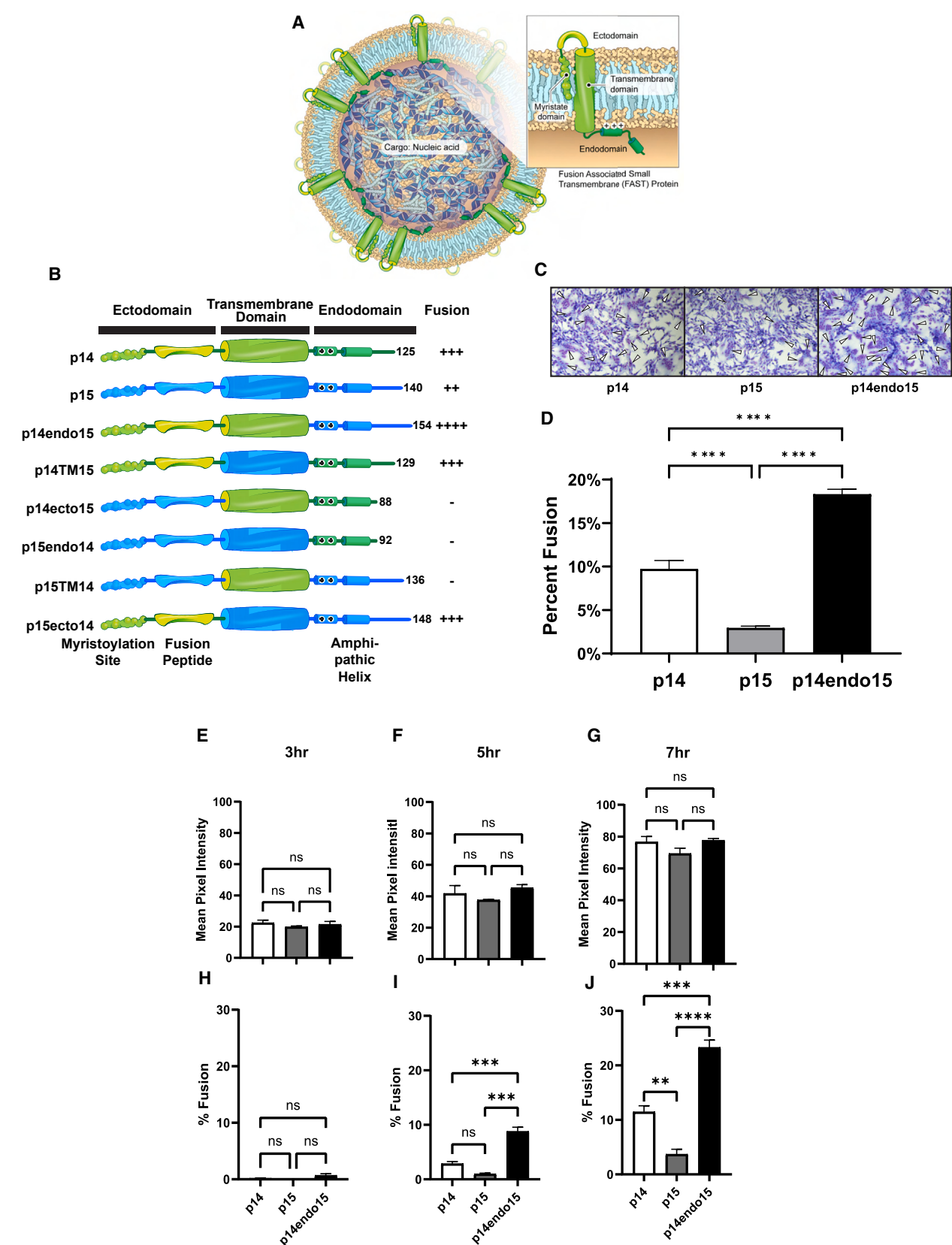
## INTRODUCTION

The potential for genetic therapies to treat illnesses ranging from monogenic disease to cancer has resulted in thousands of clinical trials and more than 10 approved nucleic acid drugs in the US alone.<sup>1</sup> Despite this, a key limitation to the wide adoption of genetic medicines is the lack of a highly tolerable, durable, and broadly distributed nucleic acid intracellular delivery platform.<sup>2</sup> The approval of alipogene tiparvovec (Glybera) to treat lipoprotein lipase deficiency in 2012 catalyzed a shift toward using adeno-associated virus (AAV) vectors for DNA delivery.<sup>3,4</sup> Although safer than many traditional viral vectors, host immunogenic responses against the AAV vector limit repeat dosing unless multiple AAV serotypes are employed.<sup>5,6</sup> Efficacy can be further limited by the existence of neutralizing antibodies with no prior AAV vector exposure.<sup>7–10</sup>

Non-viral delivery vehicles such as lipid nanoparticles (LNPs) have been widely used for RNA-based therapeutic approaches and have cost, manufacturing, and immunogenicity advantages

over viral vectors.<sup>11–19</sup> The approval of patisiran (Onpattro) as a systemic therapy<sup>19</sup> and the more recent success of LNP mRNA COVID-19 vaccines<sup>19</sup> has set the stage for the development of numerous LNP-based nucleic acid therapies. LNPs are formulated with ionizable lipids, which facilitate endosomal escape.<sup>20–23</sup> However, formulations containing ionizable lipids are also associated with tolerability challenges such as potentiation of apoptotic cell death and dose-limiting liver toxicity following systemic delivery.<sup>24–26</sup>

Given the strengths and limitations of current viral and non-viral approaches, we developed a proteolipid vehicle (PLV) platform that incorporates an engineered viral fusion protein into a lipid-based formulation to achieve intracellular delivery of nucleic acid cargoes with low immunogenicity and high tolerability. The PLV platform utilizes fusion-associated small transmembrane (FAST) proteins derived from the non-enveloped fusogenic orthoreovirus. At 100–200 residues in length, FAST proteins are the smallest known viral fusogens. These fusion proteins are expressed inside virus-infected cells and are trafficked to the



(legend on next page)

plasma membrane where they facilitate cell-cell membrane fusion, generating multinucleated syncytia to facilitate viral transmission.<sup>27,28</sup> FAST proteins function at physiological pH and do not require specific cell receptors, allowing them to fuse almost all cell types.<sup>29</sup> The FAST protein family comprises six structurally similar members named according to their molecular mass in Daltons (p10, p13, p14, p15, p16, and p22), with the rate and extent of fusion activity varying considerably between family members. While they share little conserved sequence identity, they all exhibit a bipartite membrane topology with the single transmembrane domain (TMD) connecting a minimal N-terminal ectodomain of 19–40 residues to a longer C-terminal cytoplasmic endodomain.<sup>30</sup> These motifs function in conjunction to remodel membranes and promote membrane fusion.<sup>31–37</sup>

We previously showed in proof-of-concept experiments that FAST protein-containing liposomes induce liposome-cell fusion and facilitate intracellular delivery of encapsulated membrane-impermeable cargo.<sup>29,38</sup> Here, we evaluated a panel of chimeric FAST protein constructs for fusion activity to identify a high-activity FAST protein chimera that was formulated into a PLV comprised of well-tolerated lipids (Figure 1A). We demonstrate that FAST-PLVs comprise a nucleic acid delivery platform that mediates effective delivery and expression of encapsulated mRNA and DNA *in vitro* and *in vivo*, while maintaining excellent tolerability, low immunogenicity, and favorable biodistribution in rodent and non-human primate (NHP) models.

## RESULTS

### Engineering of a FAST protein chimera with enhanced fusion activity

We exploited the modular nature of FAST proteins to determine whether a specific combination of motifs could be assembled into a recombinant FAST protein with enhanced fusion activity by substituting the ectodomain, TMD, and endodomains of the high-activity p14 and p15 FAST proteins<sup>32</sup> (Figure 1B). The fusion activity of each construct was ranked using a syncytia formation assay (Figure 1C). Three of six chimeric proteins were fusion-dead while two maintained fusion activity comparable with the parental proteins. One candidate, p14endo15, had significantly higher activity than either p14 or p15 parent (Figures 1C and 1D). This chimera comprises the p14 ectodomain and TMD with the p15 endodomain. The fusion kinetics of p14endo15

were further examined by co-transfected DNA plasmids encoding FAST protein (pDNA-FAST) as well as green fluorescent protein (pDNA-GFP) to control for transfection efficiency. While equivalent transfection and expression rates were observed for each candidate, p14endo15 FAST protein induced more rapid and extensive cell fusion, compared with parental p14 or p15 (Figures 1E–1J). Based on these results, p14endo15 was selected for the optimization of PLV formulations for nucleic acid delivery (all references to FAST protein herein describe p14endo15).

### Optimization of lipid/FAST protein formulations for nucleic acid delivery

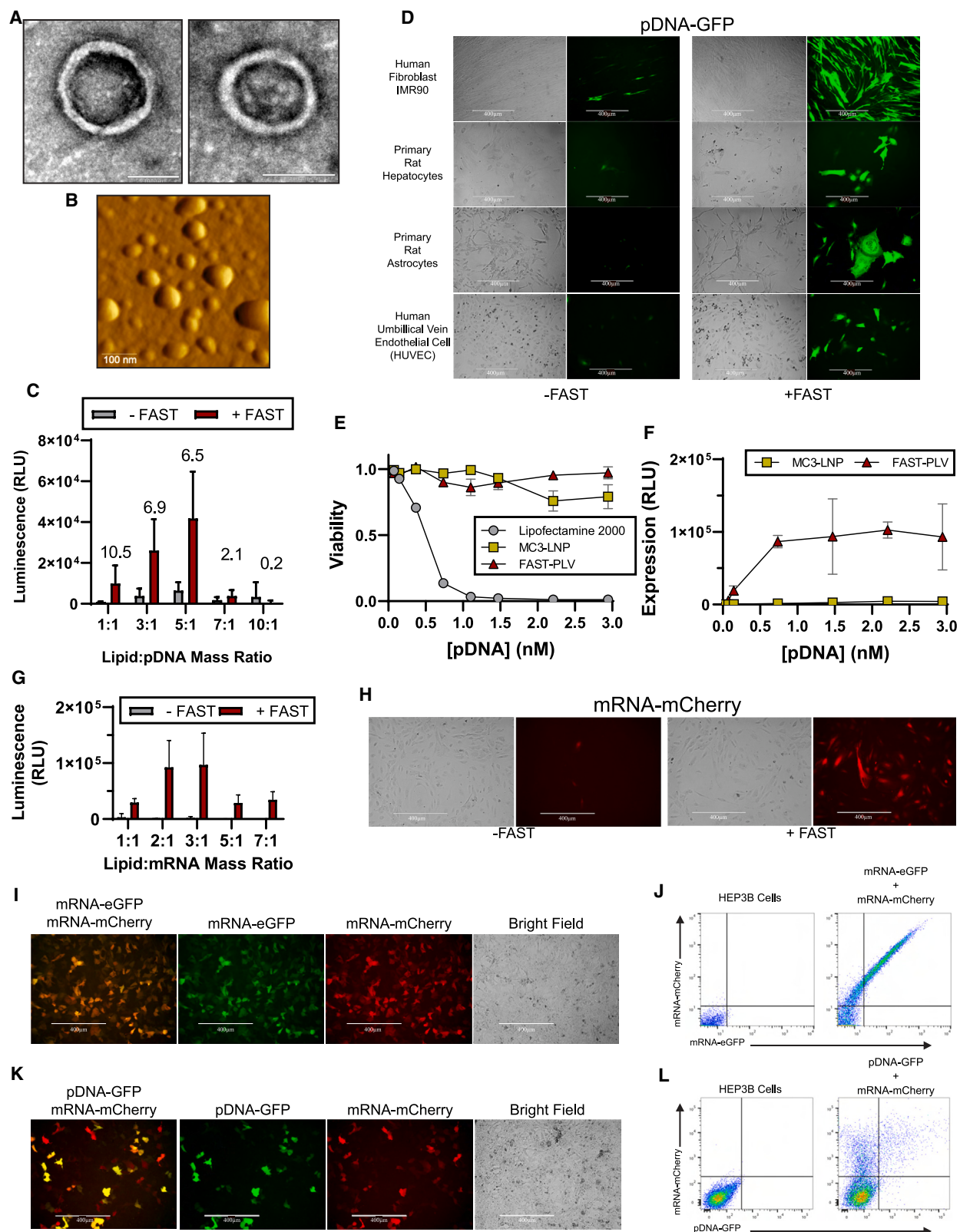
Conventional LNPs rely on endosomal escape for intracellular delivery, which limits nucleic acid release into the cytosol.<sup>13,21,39</sup> We hypothesized that incorporating p14endo15 into a lipid formulation would significantly improve the delivery of nucleic acids by promoting PLV-cell membrane fusion while avoiding endosomal escape. This would allow for increased flexibility in the lipid components because endosomal escape activity would not be required.

First, a panel of cationic and ionizable lipids was evaluated for their toxicity on human fibroblast cells (WI-38), including cationic lipids 1,2-di-O-octadecenyl-3-trimethylammonium propane (DOTMA) and 1,2-dioleoyl-3-trimethylammonium-propane (DOTAP), as well as the ionizable lipids 1,2-dioleoyl-3-dimethylammonium-propane (DODAP), DLin-MC3-DMA (MC3), and 1,2-dioleyloxy-3-dimethylaminopropane (DODMA). Of these, DODAP had the most favorable tolerability followed by DOTAP (Figure S1A). The optimal mass ratio of DODAP to pDNA was assessed by measuring the delivery and subsequent expression of DNA-encoded firefly luciferase (pDNA-Fluc) in retinal pigmented epithelial cells (ARPE-19). A ratio of 5:1 ionizable lipid DODAP to pDNA resulted in maximal expression (Figure S1B).

Next, a panel of more than 40 lipid formulations encapsulating pDNA were generated by combining DOTAP, DODAP, 2-dioleoyl-sn-glycero-3-phosphoethanolamine (DOPE), and 1,2-dimyristoyl-sn-glycero-3-methoxypolyethylene glycol-2000 (DMG-PEG) at different ratios to balance intracellular delivery and activity with tolerability. The most promising of these, based on encapsulation and sizing (designated 28M, 33T, 37N, and 41N), were produced using a microfluidic platform<sup>40–42</sup> encapsulating pDNA-FLuc with or without p14endo15 FAST protein.

**Figure 1. Engineering p14endo15 proteolipid vehicles (FAST-PLVs)**

- (A) Schematic showing the topology of a generic FAST protein in the PLV membrane and key structural motifs present in the ectodomain and endodomain.
- (B) Arrangement of the ectodomain, transmembrane domain (TMD), and endodomain fusion modules of the parental p14 and p15 FAST proteins and various chimeric constructs (p14, green; p15, blue). The locations of the N-terminal myristylation site and adjacent fusion peptide motif in the ectodomain and the endodomain polybasic motif (++) and adjacent amphipathic helix are indicated. Syncytium formation of the various constructs was scored on a 4+ scale with “–” indicating no syncytium formation.
- (C) Representative images of Giemsa-stained quail fibrosarcoma (QM5) cells transfected with pcDNA3 expressing either p14, p15, or p14endo15, captured at 13 h post-transfection. Arrows indicate syncytial nuclei.
- (D) Quantification of syncytium formation expressed as a percentage of syncytial nuclei over total nuclei. Data are represented as mean ± standard deviation,  $n = 3$ , one-way ANOVA and Tukey's multiple comparisons test.
- (E–G) QM5 cells were co-transfected with pDNA-GFP and pDNA-FAST, and mean pixel intensity of GFP is reported 3 h (E), 5 h (F), and 7 h (G) after transfection. Data are represented as mean ± standard deviation,  $n = 3$ , one-way ANOVA and Tukey's multiple comparisons test.
- (H–J) Quantification of syncytium formation in cells described in (E)–(G), with fusion expressed as a percentage of syncytial nuclei over total nuclei, 3 h (H), 5 h (I), and 7 h (J) after transfection. Data are represented as mean ± standard deviation,  $n = 3$ , one-way ANOVA and Tukey's multiple comparisons test.
- \*\* $p < 0.01$ , \*\*\* $p < 0.001$ , \*\*\*\* $p < 0.0001$ , ns = not significant.



(legend on next page)

Size, polydispersion index (PDI) and zeta potential was determined for each (Table S1). All PLV formulations were found to be  $<80$  nm in diameter with a PDI  $< 0.3$ , indicating monodispersity.

The potency and cytotoxicity of these formulations were assessed in kidney epithelial cells (Vero). Overall, formulation 41N showed the most favorable tolerability (Figure S1C) and was slightly less potent than formulation 37N (Figure S1D). A direct comparison of the potency vs. tolerability (weighted equally) indicated that formulation 41N scored higher than 37N, which in turn scored significantly higher than 28M and 33T (Figure S1E). Based on all these results, PLV formulation 41N was selected for further development and optimization.

The size and structure of the 41N FAST-PLV encapsulating pDNA was assessed by transmission electron microscopy (TEM) and atomic force microscopy (AFM). TEM revealed uniform spherical structures made of an outer lipid bilayer and a negatively stained inner core (Figure 2A). AFM showed spherical structures with an approximate size distribution of  $66.3 \pm 15.3$  nm (Figure 2B). Next, the optimal FAST protein content in PLV was determined by varying mol % levels of FAST protein and assessing transfection efficiency in a panel of cell lines. It was determined that 0.214 mol % FAST was found to generate maximal GFP expression in AC10, H1299, and HEK293T cells (Figures S2A–S2F). Cytotoxicity was then assessed by increasing FAST protein content in PLV up to 0.426 mol %, with no negative effects observed (Figures S2G–S2I). Based on this, the 41N formulation with 0.214 mol % FAST protein content was selected for further study.

Next, we examined the potency of the 41N PLV with varying ratios of ionizable lipid to pDNA-FLuc in primary human lung fibroblast cells (IMR-90) with and without FAST protein. FAST-containing formulations showed significantly higher potency, which was maximal at a 5:1 ratio of ionizable lipid to pDNA (Figure 2C). Using this 5:1 ratio, we evaluated the potency of 41N pDNA-GFP PLVs formulated with and without FAST protein in a panel of primary cell lines and observed similar results (Figure 2D). Based on this, the optimized FAST-PLV formulation was finalized using the 41N lipid formulation and a 5:1 mass ratio of DODAP to pDNA. Importantly, no evidence of cell-cell fusion or syncytia formation was observed in any of these experiments

at any PLV dose. This was examined further by transfecting H1299 cells with FAST-PLVs containing pDNA-GFP, where we observed significant GFP expression with no evidence of syncytia formation. Transfection using pDNA-FAST, in contrast, demonstrated significant syncytia formation (Figure S3).

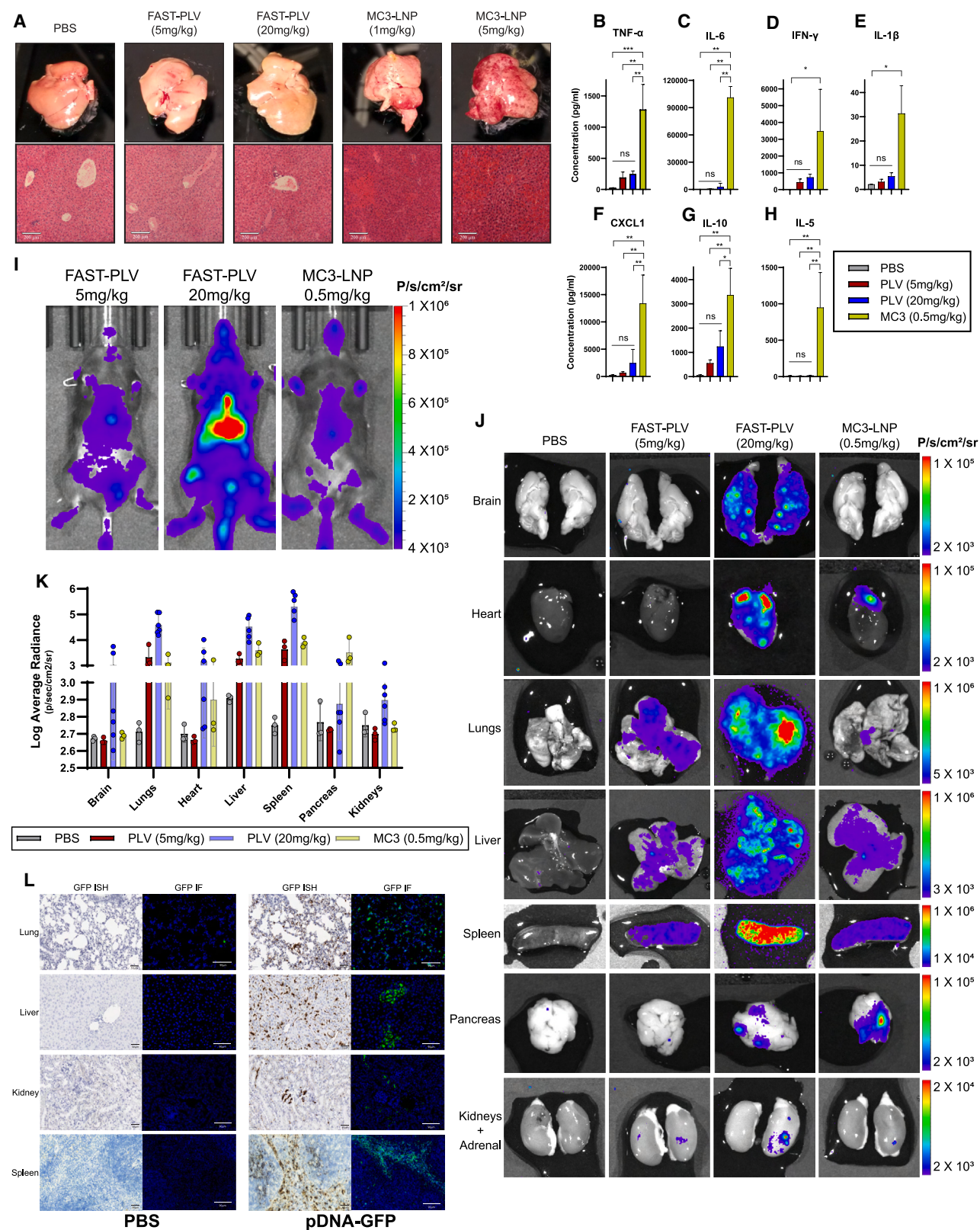
To establish a suitable reference point, we compared the potency and tolerability of FAST-PLVs to the cationic lipid formulation Lipofectamine 2000 and a conventional LNP formulation composed of DLin-MC3-DMA (MC3-LNPs) in human umbilical vein endothelial cells (HUVECs) and IMR-90.<sup>24</sup> FAST-PLVs and MC3-LNPs containing pDNA-FLuc were significantly less toxic than Lipofectamine 2000 (Figure 2E), with FAST-PLVs demonstrating significantly higher luminescence than MC3-LNPs (Figure 2F).

The delivery of mRNA in the 41N PLV formulation with and without FAST protein was then assessed using a range of mass ratios of DODAP to mRNA. The highest expression of mRNA-FLuc in WI-38 cells was found at a DODAP:mRNA ratio of 3:1, and the incorporation of FAST protein significantly enhanced potency (Figure 2G). Similar results were also seen with the delivery of mRNA-mCherry into HUVEC, where the incorporation of FAST protein significantly increased mCherry expression (Figure 2H). The ability of FAST-PLVs to deliver multiple mRNAs to the same cell was demonstrated by co-expression of mRNA-mCherry and mRNA-eGFP in cells treated with PLVs containing a 1:1 molar ratio of each mRNA (Figures 2I and 2J). Furthermore, FAST-PLVs formulated with a mixture of pDNA-GFP and mRNA-mCherry cargo at a 1:6 molar ratio demonstrated expression of both reporters in cells (Figures 2K and 2L). Thus, the optimized FAST-PLV formulation is suitable for encapsulation and intracellular delivery of pDNA and/or mRNA to cultured cells with a high potency and low toxicity.

To confirm that FAST-PLVs deliver nucleic acids through an endocytosis-independent mechanism, as previously observed,<sup>29</sup> we assessed the delivery of Cy5-conjugated hypoxanthine-guanine phosphoribosyltransferase-1 (HPRT1) small interfering RNA (siRNA) into ARPE-1 cells, using FAST-PLVs, compared with MC3-LNPs. Confocal microscopy confirmed that siRNA delivered by MC3-LNPs primarily localize to Rab5a-positive<sup>43–45</sup> early endosomes after 1 h. Delivery of siRNA by FAST-PLV resulted in diffuse cytoplasmic and punctate localization and little to no

#### Figure 2. *In vitro* validation of FAST-PLVs

- (A and B) FAST-PLVs encapsulating pDNA were imaged with (A) transmission electron microscopy and (B) atomic force microscopy.
- (C) ARPE-19 cells were incubated with pDNA-FLuc encapsulated within optimized lipid formulation 41N with and without FAST protein at different ionizable lipid:pDNA mass ratios for 96 h before luminescence was determined. Data are represented as mean  $\pm$  standard deviation,  $n = 3$ .
- (D) Optimized lipid formulation 41N with (right) and without (left) FAST protein was used to encapsulate pDNA-GFP, and 0.9 nM was incubated for 96 h before fluorescence images were taken.
- (E) Viability of HUVECs treated with varying amounts of pDNA encapsulated in Lipofectamine 2000, MC3-LNPs, and FAST-PLVs. Data are represented as mean  $\pm$  standard deviation,  $n = 5$ .
- (F) Expression of pDNA-FLuc in IMR-90 cells delivered by MC3-LNPs or FAST-PLVs. Data are represented as mean  $\pm$  standard deviation,  $n = 5$ .
- (G) *In vitro* expression of mRNA-FLuc encapsulated within optimized lipid formulation 41N at multiple ionizable lipid:mRNA mass ratios made with and without FAST protein 48 h after addition to WI-38 cells. Data are represented as the mean  $\pm$  standard deviation,  $n = 5$ .
- (H) Optimized lipid formulation 41N with and without FAST protein was used to encapsulate mRNA-mCherry at the optimal 3:1 mass ratio and incubated with HUVECs for 48 h before fluorescence images were taken.
- (I) HEP3B cells were incubated with FAST-PLVs encapsulating 6 nM mRNA-eGFP and 6 nM mRNA-mCherry for 48 h before fluorescence images were taken.
- (J) Flow cytometry conducted on cells from (I).
- (K) HEP3B cells were incubated with FAST-PLVs encapsulating 1 nM pDNA-GFP and 6 nM mRNA-mCherry for 72 h before fluorescence images were taken.
- (L) Flow cytometry conducted on cells from (K).
- See also Figures S1, S2, S3, and S4.



(legend on next page)

observable early endosome co-localization (Figure S4A). Next, we assessed the impact of the endocytosis inhibitor dynasore on the delivery of siRNA-Cy5.<sup>46,47</sup> Dynasore (125 μM) significantly reduced the internalization of AF488-labeled epidermal growth factor (EGF) in ARPE-1 cells<sup>48–50</sup> (Figures S4B–S4D). Next, we examined the effect of dynasore at 125 μM on the uptake of siRNA-Cy5 encapsulated within PLVs with and without FAST protein. FAST proteins significantly increased the intracellular uptake of siRNA-Cy5 in the presence or absence of dynasore (Figures S4E–S4G). Dynasore inhibited delivery by 85% in the absence of FAST protein and only by 45% when FAST protein was included (Figures S4E–S4G), indicating significant non-endosomal uptake. We then examined the activation of the cyclic GMP-AMP synthase (cGAS), stimulator of interferon genes (STING) pathway to assess intracellular DNA delivery<sup>51–53</sup> by transfecting H1299 cells with pDNA-GFP in MC3-LNP, FAST-PLV, or with Lipofectamine 2000. We observed no cGAS-STING activation with MC3-LNPs, presumably due to the DNA remaining trapped in the endosome. FAST-PLVs induced a small but significant increase in cyclic guanosine monophosphate–adenosine monophosphate (cGAMP) levels, confirming the presence of pDNA in the cytoplasm. Transfection with Lipofectamine 2000 resulted in high cGAMP levels, likely due to significant deposition of pDNA in the cytoplasm<sup>54</sup> (Figure S4H). Overall, these results support an endosomal-independent mechanism for the intracellular delivery of nucleic acids by FAST-PLV.

### Systemic *in vivo* delivery of pDNA via FAST-PLVs

Safe and effective systemic delivery of DNA is a significant challenge, with many platforms exhibiting low tolerability *in vivo*.<sup>39,55,56</sup> We evaluated the *in vivo* biodistribution, potency, and tolerability of FAST-PLVs, compared with MC3-LNPs, over a dose range of 0.5–80 mg/kg DNA. Systemic intravenous administration of MC3-LNPs encapsulating pDNA-FLuc at doses higher than 1 mg/kg resulted in significant mortality of mice, while FAST-PLVs were well tolerated at doses >60 mg/kg (Table S2). Post-mortem analysis of MC3-LNP-treated mice at 1 and 5 mg/kg revealed significant liver toxicity characterized by hemorrhage. In contrast, mice treated with FAST-PLVs at doses up to 20 mg/kg showed no signs of liver pathology by gross visual or histological examination (Figure 3A). Cytokine responses in mice were also examined as an immune indicator of toxicity<sup>57</sup> following intravenous injection. Mice receiving 5 and 20 mg/kg of FAST-PLVs encapsulating pDNA-

FLuc had no significant increase in any of the measured cytokines, while all measured pro-inflammatory cytokines were significantly elevated in mice treated with MC3-LNPs encapsulating 0.5 mg/kg pDNA-FLuc (Figures 3B–3H).

Next, the *in vivo* potency and biodistribution of FAST-PLVs, compared with MC3-LNPs, were evaluated using whole-animal luminescence and ex vivo imaging after systemic administration of pDNA-FLuc. Owing to tolerability limitations, MC3-LNPs were assessed at a 0.5 mg/kg dose, while FAST-PLVs were assessed at 5 and 20 mg/kg. A significant increase in FLuc expression between the 5 and 20 mg/kg FAST-PLV doses was observed with broad biodistribution (Figure 3I). A more detailed comparison by ex vivo bioluminescence imaging indicated that the 5 mg/kg dose of FAST-PLVs produced comparable FLuc expression in multiple organs to 0.5 mg/kg MC3-LNP, while the higher 20 mg/kg dose of FAST-PLV resulted in substantially higher FLuc expression: 13-fold higher in the liver, 20-fold higher in the lungs, 30-fold higher in the spleen, 1.5-fold higher in the kidneys, 3.5-fold higher in the brain, and 3-fold higher in the heart (Figures 3J and 3K).

Next, we assessed biodistribution and expression at the cellular level after systemic administration of FAST-PLVs encapsulating 20 mg/kg pDNA-GFP. 24 h after injection significant GFP mRNA expression in the lungs, liver, kidneys, and spleen was detected by *in situ* hybridization (RNAscope) (Figure 3L). Immunofluorescence confirmed expression of GFP protein throughout these organs, with expression throughout the pulmonary alveoli and in liver hepatocytes. GFP expression was predominately observed in the proximal tubules of kidney. In the spleen, most of the GFP expression was observed in the red pulp with modest expression detected in the white pulp (Figures 3L and S5). The durability of *in vivo* pDNA expression was also assessed by whole-body luminescence imaging over 365 days after systemic administration of 20 mg/kg pDNA-FLuc FAST-PLV. A strong and widespread whole-body luminescence signal was observed in the first 2 days, which decreased to a steady state that was maintained through 1 year after administration (Figure S6).

Batch-to-batch manufacturing consistency was maintained by implementing strict biophysical release criteria that included size (number) <80 nm, PDI < 0.3, and encapsulation efficiency >80%. To support these criteria, we compared the functionality and physical characteristics of two FAST-PLV batches encapsulating pDNA-FLuc manufactured on different days.

### Figure 3. Delivery of pDNA by FAST-PLVs in mice

(A) Post-mortem liver images and hematoxylin and eosin staining of liver sections from mice injected with multiple doses of FAST-PLVs or MC3-LNPs encapsulating pDNA-FLuc (magnification = 10x).

(B–H) Serum concentrations of pro-inflammatory cytokines: (B) tumor necrosis factor alpha (TNF-α), (C) interleukin (IL)-6, (D) interferon (IFN)-γ, (E) IL-1β, (F) chemokine ligand 1 (CXCL1), (G) IL-10, and (H) IL-5; 24 h after injection with PBS, MC3-LNPs, or FAST-PLVs encapsulating pDNA-FLuc. Data are represented as mean ± standard deviation, n = 3 biologically independent mice per group, one-way ANOVA and Tukey's multiple comparisons test.

(I) Whole-body bioluminescent imaging of mice 24 h after injection with pDNA-FLuc encapsulated within MC3-LNPs or FAST-PLVs.

(J) Ex vivo organ bioluminescence from mice 24 h after intravenous injection with pDNA-FLuc.

(K) Quantification of bioluminescent signal from ex vivo organs presented in (J). Values presented as log<sub>2</sub> of average radiance. Data are represented as mean ± standard deviation.

(L) GFP *in situ* hybridization (RNAscope) and GFP immunofluorescence conducted 24 h after intravenous injection with PBS or FAST-PLVs encapsulating 20 mg/kg pDNA-GFP (magnification = 20x).

\*p < 0.05, \*\*p < 0.01, \*\*\*p < 0.001, \*\*\*\*p < 0.0001, ns = not significant.

See also Figures S5, S6, and S7.

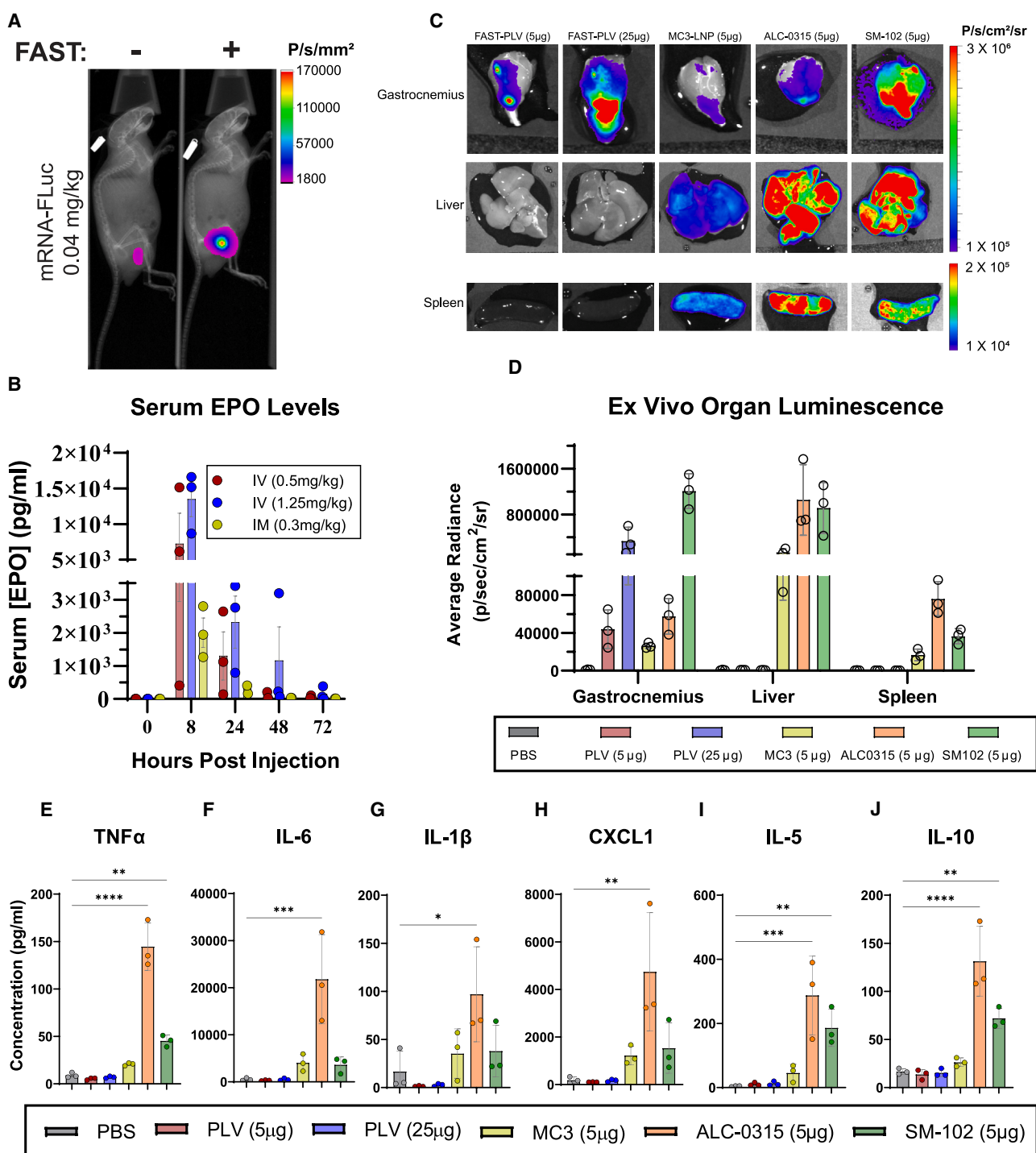


**Figure 4. Comparison of mRNA delivery by FAST-PLVs to conventional LNP platforms**

(A) Intramuscular injection of 41N formulation encapsulating mRNA-FLuc with and without FAST protein.

(B) Serum EPO concentrations following intravenous or intramuscular injection with FAST-PLVs encapsulating mRNA-EPO. Data are represented as mean ± standard deviation,  $n = 3$  biologically independent mice per group.

(C) Ex vivo organ bioluminescence from mice 24 h after intramuscular injection into the gastrocnemius muscle with mRNA-FLuc encapsulated within FAST-PLVs, MC3-LNPs, ALC-0315 LNPs, or SM-102 LNPs.

(D) Quantification of bioluminescent signal from ex vivo organs in (C). Data are represented as mean ± standard deviation,  $n = 3$  biologically independent mice per group.

(legend continued on next page)

Biophysical characteristics of both batches were comparable (Figures S7A–S7C), as well as whole-body luminescence signal (Figures S7D–S7F).

### In vivo delivery of mRNA formulated in FAST-PLVs

Next, we assessed the ability of FAST-PLVs to deliver mRNA *in vivo*. Incorporation of FAST protein into mRNA-FLuc PLVs resulted in significantly increased expression following intramuscular injection (Figures 4A and S8A). We then examined the ability of FAST-PLVs to deliver therapeutic mRNA cargo via intramuscular and intravenous injection. 8 h after administration we observed a large spike in serum erythropoietin (EPO) levels following systemic FAST-PLV administration reaching 7,000 and 13,000 pg/mL in mice injected with the 0.5 and 1.25 mg/kg doses of mRNA-EPO, respectively.<sup>13,17,26,58</sup> Intramuscular administration with 0.3 mg/kg mRNA-EPO resulted in a serum EPO concentration approaching 2,000 pg/mL 8 h following administration (Figure 4B).

We then compared the delivery of mRNA in FAST-PLVs to clinically approved LNP formulations developed by Alnylam, Pfizer, and Moderna (using the MC3, ALC-0315, and SM-102 ionizable lipids, respectively) by intramuscular administration in immune-competent mice. A dose of 5 µg of mRNA-FLuc was selected for comparison, and a 25 µg dose was added for FAST-PLVs owing to their improved safety profile. Expression in the injected gastrocnemius (GAS) muscle at the 5 µg dose was similar for FAST-PLVs, MC3, and ALC-0315 LNPs. Substantially higher muscle expression was observed for the SM102 LNP and with the higher 25 µg dose of FAST-PLV. Expression was restricted to the injected muscle in mice injected with FAST-PLVs, even at the higher 25 µg dose. For the three clinically approved LNPs, we observed substantial luciferase expression in both liver and spleen (Figures 4C and 4D). Given the differences in biodistribution, we then examined the impact on the systemic induction of pro-inflammatory cytokines. FAST-PLVs did not induce any increase in pro-inflammatory cytokines at either the 5 or 25 µg dose, while ALC-0315- and SM-102-formulated LNPs resulted in significant increases in the levels of several circulating pro-inflammatory cytokines (Figures 4E–4J).

Next, we assessed delivery of mRNA-FLuc in FAST-PLVs, compared with MC3-LNPs, by several other routes of administration including intrathecal, intracerebral ventricular, and intravittreal injection. Intrathecal administration of FAST-PLVs resulted in luciferase expression that was restricted to the spinal cord and head by whole-body luminescence imaging, whereas delivery of MC3-LNPs resulted in significant reporter expression outside the CNS (Figure S9A). Ex vivo luminescence imaging confirmed that MC3-LNPs resulted in substantial liver and spleen luciferase expression, while FAST-PLVs resulted in expression only in the brain (Figures S9B and S9C). Similar characteristics were observed after intracerebral ventricular administration (Figures S9D–S9F). Intravittreal administration of FAST-PLVs resulted in significant luciferase

expression in the eye (Figures S9G–S9I), with ex vivo imaging demonstrating that the bulk of expression is coming from the back of the eye where the retina is located (Figure S9H). Significant off-target liver and spleen luciferase expression was observed in mice injected with MC3-LNPs (Figures S9G–S9I). Taken together, these results demonstrate that FAST-PLV formulations drive robust expression in the local area or organ subsequent to localized administration of mRNA to the muscle, brain, or eye. In contrast, current clinically approved LNP formulations result in substantial off-target liver and spleen expression.

We then assessed the biodistribution and expression of mRNA-FLuc at a 0.5 mg/kg dose in FAST-PLVs, compared with MC3-LNP, after systemic administration. The MC3-LNP-injected animals showed expression that was mainly restricted to liver and spleen, while FAST-PLVs demonstrated substantially lower liver expression and significant extrahepatic expression in the lungs, spleen, brain, heart, and kidneys (Figures 5A and 5B). An analysis of tissue/liver expression indicated mice receiving FAST-PLVs showed higher expression in the brain, lungs, heart, and spleen, compared with the liver, while MC3-LNP expression was highly liver-tropic (Figure 5C).

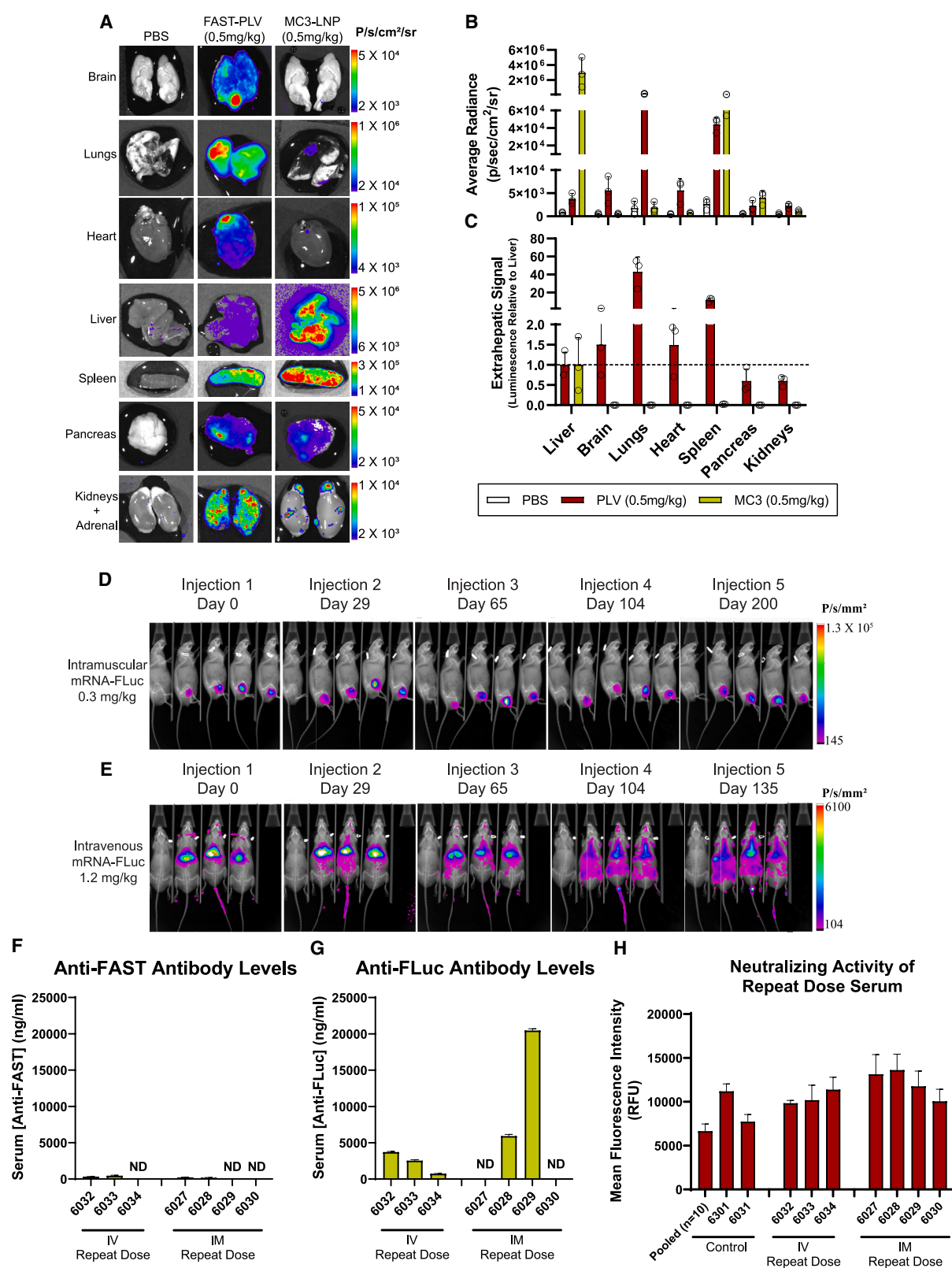
### Repeat dosing of FAST-PLVs through intramuscular or systemic route

Administered biologic drugs such as viral vectors elicit an adaptive immune response in the form of anti-vector antibodies that can interfere with or neutralize the effect of the vector, restricting their use in applications that require repeat dosing.<sup>5,8,9</sup> Given the incorporation of a novel virus-derived fusion protein in our FAST-PLV platform, we sought to determine if FAST-PLVs generate an immune response capable of reducing *in vivo* efficiency upon repeated administration. To that end, FAST-PLVs encapsulating mRNA-FLuc were administered at 0.3 mg/kg intramuscularly or 1.2 mg/kg intravenously once per month for 6 months. Significant luciferase expression was seen after each intramuscular injection (Figures 5D, S8B, and S8C). When FAST-PLVs were repeatedly administered intravenously, no significant change in total luminescence intensity was observed over time (Figures 5E, S8D, and S8E). Antibodies against FAST protein were quantified in the serum of these mice 1 month after the final FAST-PLV administration. Two intramuscularly injected animals and one intravenously injected animal had anti-FAST antibody levels below the lower limit of quantification (Figure 5F). Interestingly, high titers of anti-FLuc antibodies were detected in several of the repeatedly dosed animals (Figure 5G). To determine whether the detected levels of anti-FAST antibodies have neutralizing activity, the activity of pDNA-GFP PLVs in the presence of serum from repeatedly dosed and control mice was assessed in an *in vitro* transfection assay. No reduction in GFP expression was observed when serum-treated FAST-PLVs were used to transfet 3T3 cells *in vitro* (Figure 5H), indicating no neutralizing activity. Overall, repeat dosing of FAST-PLVs

(E–J) Serum concentrations of pro-inflammatory cytokines: (E) TNF- $\alpha$ , (F) IL-6, (G) IL-1 $\beta$ , (H) CXCL1, (I) IL-5, and (J) IL-10. 6 h after injection with PBS, or mRNA-FLuc encapsulated within FAST-PLVs, MC3-LNPs, ALC-0315 LNPs, and SM-102 LNPs. Data are represented as mean  $\pm$  standard deviation,  $n = 3$  biologically independent mice per group, one-way ANOVA and Tukey's multiple comparisons test.

\* $p < 0.05$ , \*\* $p < 0.01$ , \*\*\* $p < 0.001$ , \*\*\*\* $p < 0.0001$ .

See also Figures S8 and S9.



(legend on next page)

by intramuscular or intravenous administration produced consistent reporter expression, was well tolerated, and did not stimulate adverse immune responses.

### FAST-PLVs safely and effectively deliver pDNA in NHPs with broad biodistribution to tissues

The safety, tolerability, and biodistribution of FAST-PLVs at various doses following systemic administration were further examined in African green monkeys (*Chlorocebus sabaeus*). The biodistribution of an inert pDNA cargo delivered by intravenous administration in FAST-PLVs at a 1 mg/kg dose of pDNA was quantified in 30 tissues, using a quantitative PCR approach, 2 days after administration. Significant levels of pDNA were detected in all organs tested, with the highest levels detected in the lungs, spleen, gall bladder, and bone marrow. These organs all demonstrated higher uptake than liver, supporting the fact that PLV is suitable for extrahepatic delivery of pDNA (Figure 6A).

We then evaluated tolerability following intravenous administration with FAST-PLVs at 1 and 6 mg/kg pDNA doses. No significant abnormalities were observed in any organs assessed (Figure 6B), and no treatment-related changes were noted in any organs tested (Table S3). Some findings were reported in all animals in the aged, feral African green monkey cohort used for the study. For example, the mononuclear cell infiltrates observed in the livers of all animals, as well as the vacuolation and hydropic degeneration, were within normal variability for African green monkeys. Additionally, the periportal hemosiderin and pigmented macrophages detected are typical of prior parasite migration tracks—consistent with the use of wild-caught animals.<sup>59,60</sup> Circulating levels of alanine transaminase (ALT) and aspartate transaminase (AST) remained within the normal range for the duration of the study. Creatine phosphokinase (CPK) and lactate dehydrogenase (LDH) levels were elevated immediately following infusion but decreased to normal range by 21 days post-infusion. All other clinical chemistry parameters remained within the normal range for the study duration (Table S4). A transient elevation in systemic pro-inflammatory cytokines was observed 1–4 h after FAST-PLV infusion, which returned to baseline 12–72 h post-infusion (Table S5). A similar pattern was observed on chemokine secretion after FAST-PLV infusion, with chemokines returning to baseline values within 72 h after infusion (Table S6). Elevations in cytokine and chemokines were not dose dependent, suggesting factors related to the intravenous infusion, such as local

inflammation, might be the principle contributing factor. Serum levels of S protein-bound C-terminal complex (SC5b-9) did not increase significantly following FAST-PLV infusion (Figure 6C), while serum levels of C4d were elevated approximately 3-fold by the 1 mg/kg dose but were unaffected by the 6 mg/kg dose (Figure 6D).<sup>61,62</sup> The lack of a dose-dependent response indicates that it is unlikely that the administration of FAST-PLVs is responsible for this elevation.

The presence of anti-FAST antibodies was also assessed in these animals at 25 days post-administration of 6 mg/kg pDNA FAST-PLVs. Anti-FAST antibodies were only detected in one of the three monkeys at a level of  $144.72 \pm 13.5$  ng/mL. To determine whether the detected levels of anti-FAST antibodies have neutralizing activity, the activity of pDNA-GFP PLVs in the presence of baseline or day-25 serum was assessed, and no reduction in GFP expression was observed when serum-treated FAST-PLVs were used to transfect 3T3 cells *in vitro* (Figure S10). Taken together, these data indicate that FAST-PLVs are safe and well tolerated in NHPs, with broad biodistribution and extrahepatic delivery of pDNA.

### Therapeutic activity of FAST-PLV FST gene therapy

To determine the ability of FAST-PLVs to deliver pDNA encoding a therapeutic cargo, we developed a gene therapy approach to elevate expression of the protein follistatin (FST). FST facilitates hypertrophy of skeletal muscle by exhibiting an antagonistic effect on myostatin and is being examined as a potential treatment for muscle wasting disorders.<sup>63–65</sup> We sought to determine if delivery of pDNA encoding the FST-344 splice variant in FAST-PLV would be a viable alternative to AAV-based therapies. When FAST-PLVs encapsulating pDNA-FST were incubated with C2C12 mouse myoblasts, robust FST expression was observed over 3 days, with an increase in Akt and mTOR phosphorylation 24 and 48 h after addition of pDNA-FST (Figure 7A).<sup>66</sup> FST presence in the growth media also increased in a time-dependent manner (Figure 7B).

Next, we examined the ability of systemically administered FAST-PLVs to drive FST expression *in vivo*. As FST is primarily produced in the liver, we evaluated expression when driven by the liver promoter, transthyretin (TTR).<sup>67</sup> Intravenous administration of a single 10 mg/kg dose of pDNA-TTR-FST encapsulating FAST-PLVs in mice resulted in a significant spike in serum FST concentration 1 day after injection. These values returned to

### Figure 5. Systemic delivery of mRNA by FAST-PLVs in mice

- (A) *Ex vivo* organ bioluminescence of mice 5 h after intravenous injection with PBS or mRNA-FLuc encapsulated within FAST-PLVs or MC3-LNPs
- (B) Quantification of bioluminescent signal from *ex vivo* organs presented in (A). Data are represented as mean  $\pm$  standard deviation,  $n = 3$  biologically independent mice per group.
- (C) Average radiance values of organs presented in (B) are normalized to average radiance of the liver to determine extrahepatic signal.
- (D) Mice repeatedly dosed intramuscularly with 0.3 mg/kg mRNA-FLuc encapsulated within FAST-PLVs, once a month for 6 months. The first mouse is a control injected with PBS.
- (E) Mice repeatedly dosed intravenously with 1.2 mg/kg mRNA-FLuc encapsulated in FAST-PLVs, once a month for 6 months. The first mouse is a control injected with PBS.
- (F) Anti-FAST antibody levels in the serum. ND = not detected.
- (G) Anti-FLuc antibody levels in the serum. ND = not detected.
- (H) Serum from repeatedly dosed mice was incubated with FAST-PLVs encapsulating pDNA-GFP prior to addition to 3T3 cells. Flow cytometry was conducted 96 h after addition, and mean fluorescence intensity of the GFP<sup>+</sup> population is presented. Pooled serum is a combination of equivalent volumes of serum from 10 separate animals.
- See also Figure S8.

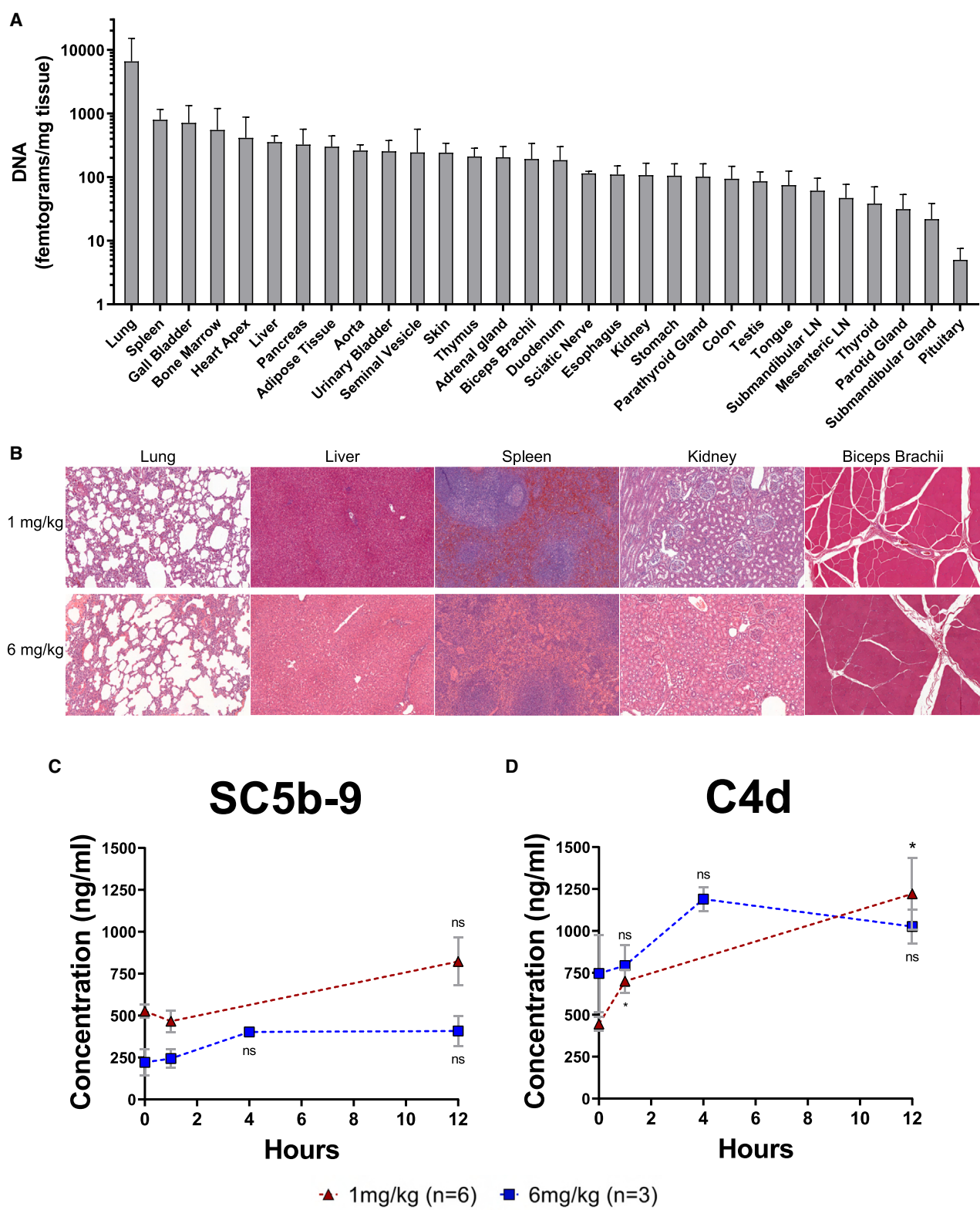


**Figure 6. Validation of FAST-PLVs safety in non-human primates**

(A) pDNA levels in organs from adult green monkeys (*Chlorocebus sabaeus*) 2 days after infusion with FAST-PLVs encapsulating 1 mg/kg pDNA.  $n = 3$  biologically independent primates.

(legend continued on next page)

near baseline levels 7 days following administration (Figure 7C). After 15 weeks, FST gene therapy resulted in animals displaying a fuller frame and musculature relative to PBS-injected control (Figure S11A). Mice receiving FST gene therapy displayed significantly higher body weight (Figures 7D and S11B) and grip strength (Figures 7E and S11C), compared with PBS control mice. At 34 weeks post-injection, gross dissection displayed an increase in muscle size in mice receiving FST gene therapy, particularly in the hind limb and throughout the torso (Figure 7F). GAS muscles isolated from FST-treated mice weighed significantly more than those isolated from PBS-injected mice (Figure 7G). Wheat germ agglutinin (WGA) staining of GAS muscle indicated significant increases in cross-sectional muscle fiber area (Figures 7H and 7I).

## DISCUSSION

PLVs formulated with FAST proteins represent an effective and redosable nucleic acid delivery platform that enables broad biodistribution with high tolerability, compared with conventional non-viral approaches. The discovery of a novel and highly active chimeric FAST fusogen, p14endo15, has enabled the re-imaging of the conventional LNP formulation to remove cholesterol, utilize alternative ionizable lipids, and select an optimal ratio of ionizable, helper, and PEGylated lipids to achieve these characteristics. The superior fusion activity of p14endo15 is mediated by the p14 ectodomain fusion peptide and myristate moiety facilitating lipid mixing with the target cell membrane, followed by the p15 endodomain fusion-inducing lipid packing sensor (FLiPs) motif partitioning into the PLV membrane to promote pore formation and PLV-cell fusion activity.<sup>35,68</sup>

Systemic *in vivo* administration of pDNA FAST-PLVs resulted in durable, dose-dependent expression of target proteins in a wide array of organs, with no detectable tissue or immune toxicity, even at doses orders of magnitude higher than the maximum tolerated dose of clinically approved LNPs. Conventional LNPs accumulate preferentially in the liver when administered systemically, mediated by ApoE binding to the LNP surface. This behavior has driven the clinical development of liver-targeting siRNA-based LNP drugs,<sup>19,69</sup> while limiting their broader application. Extrahepatic nucleic acid delivery is particularly important for indications such as cancer, which requires broad biodistribution to achieve sufficient uptake.<sup>4</sup> We found that this liver-tropic pattern was also observed with LNPs after administration in the CNS or in the eye. The mechanism behind this marked liver-homing effect is not clear but is likely mediated by cholesterol, which is a significant constituent of LNPs but not FAST-PLVs.<sup>70</sup> Like LNPs, most AAV serotypes tend to preferentially target the liver.<sup>64,71</sup> This creates problems for other conditions, as gene transfer may require local AAV delivery that is not possible for all conditions.<sup>72</sup> Additionally, cells with a high turnover rate will quickly dilute the transgene, and due to immunogenic responses, the vector cannot be

utilized again.<sup>73–76</sup> This creates problems for the development of genetic medicines targeting disseminated cancer. Based on our mouse and NHP biodistribution data that demonstrates quite extensive extrahepatic delivery of pDNA and mRNA, we anticipate that FAST-PLVs will have substantial clinical utility in the treatment of advanced cancer.

The ability of FAST-PLVs administered systemically to deliver pDNA encoding FST-344, and for gene delivery to effect quantifiable changes in muscle tissue similar to previous reports with AAV, demonstrates the potential clinical utility of this non-viral platform.<sup>77–80</sup> Again, the low immunogenicity of FAST-PLVs is beneficial for this type of gene therapy. Where AAV essentially requires lifelong gene expression with a single dose, FAST-PLV administration can be adjusted to fit each patient's need. The successful *in vivo* delivery of pDNA, using FAST-PLVs described herein, represents a promising step forward for the development of non-viral gene therapy approaches.<sup>4,39</sup> Typically, non-viral delivery vectors, such as LNPs, are only suitable for RNA-based gene therapy approaches owing to challenges encapsulating large molecules like DNA.<sup>39</sup>

While promising results have been obtained with AAV vectors, their small cargo capacity and anti-AAV immune responses limit their use.<sup>9,81–83</sup> The large cargo capacity of FAST-PLVs indicate potential for the development of CRISPR-Cas9 gene editing technologies.<sup>83,84</sup> Successful gene editing requires delivery of both Cas9 protein and a guide RNA (gRNA) to the target cell. Cas9 transgenes are approximately 4.2 kb, which puts them at the upper end of AAV packing capacity.<sup>85</sup> Utilizing FAST-PLVs would enable both Cas9 and gRNA sequences to be included on a single pDNA. Alternatively, Cas9 and gRNA could be co-encapsulated into the same PLV, which would enable the use of either pDNA or mRNA or a combination of both.

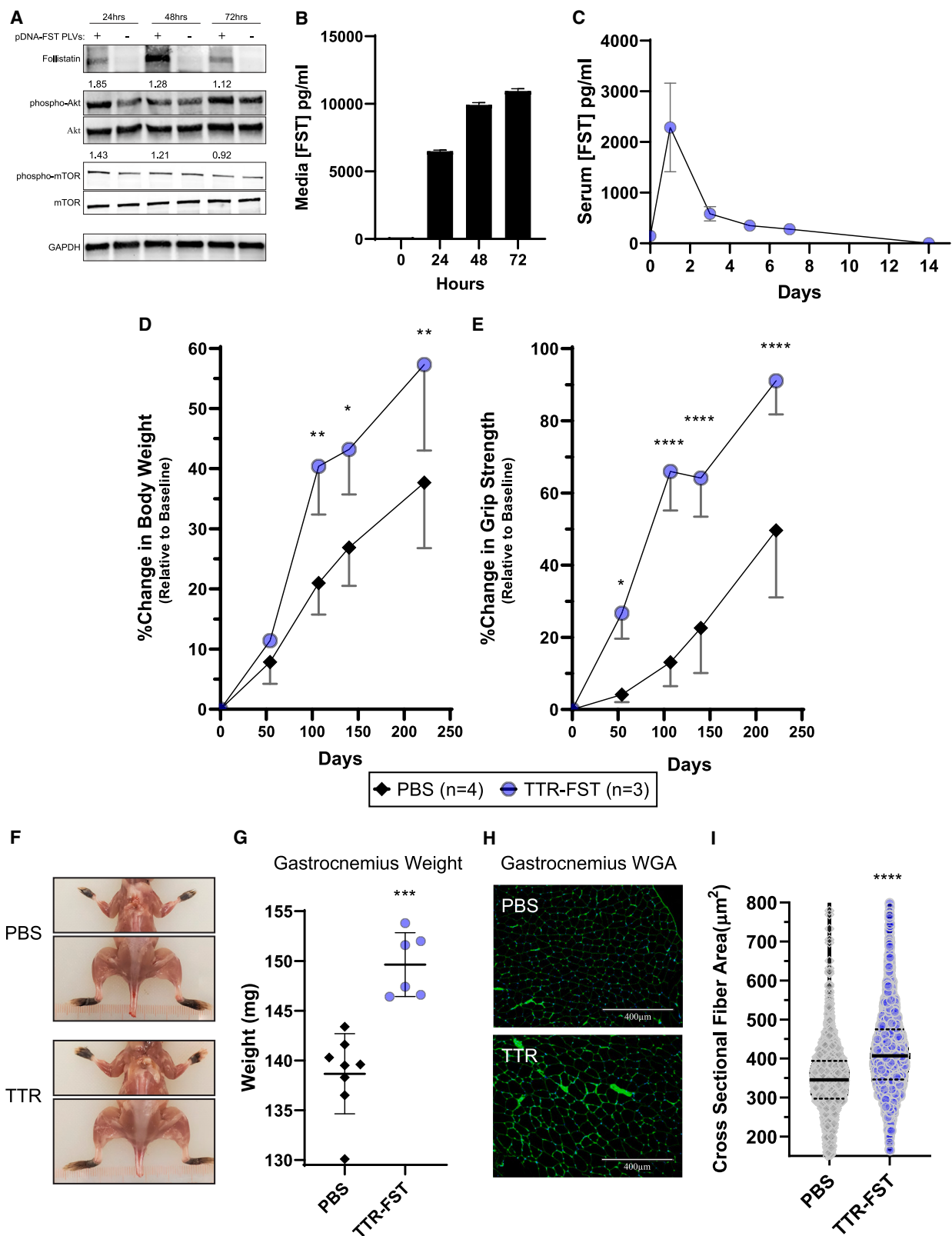
The recent development, manufacture, and production of the highly effective LNP-formulated mRNA vaccines against SARS-CoV-2 have validated the LNP platform and shown the potential of nucleic acid for vaccines and therapeutics.<sup>86–90</sup> These formulations resulted in significant transgene expression in the liver and spleen, following intramuscular injection, and facilitated a robust cytokine response, which is likely partially responsible for their efficacy as a vaccine platform. The potential for nanoparticle encapsulated DNA vaccines has been overlooked primarily owing to the high toxicity associated with cationic lipids, necessitating the use of physical methods like electroporation to deliver the DNA vaccine.<sup>91–95</sup> Our findings suggest that FAST-PLVs could also be used to deliver mRNA or DNA vaccines, avoiding the immunogenicity and toxicity seen with cationic LNP delivery platforms and the necrosis and widespread tissue damage observed with electroporation.<sup>91,96–100</sup>

In summary, we present an approach to achieve systemic nucleic acid delivery by combining the fusion-inducing activities of FAST proteins with the improved safety and scalability of lipid-based non-viral delivery vectors. Given the small size of FAST-

(B) Representative hematoxylin and eosin images 1 day after intravenous infusion with FAST-PLVs encapsulating 1 or 6 mg/kg pDNA (magnification = 10 $\times$ ). (C and D) Serum levels of (C) SC5b-9 and (D) C4d after FAST-PLV infusion. Data are represented as mean  $\pm$  standard deviation,  $n = 3$  biologically independent primates per group, two-way ANOVA and Sidak's multiple comparisons test.

\* $p < 0.05$ , ns = not significant.

See also Figure S10.



(legend on next page)

PLVs, as well as their efficacy, low immunogenicity, high tolerability, and the ability to reach extrahepatic tissues, we anticipate that FAST-PLVs will have substantial clinical utility, enabling the development of low-cost genetic medicines in the near future.

### Limitations of the study

In this study, we demonstrate delivery of mRNA and pDNA by using the FAST-PLV platform and several routes of administration, resulting in expression in a wide range of tissues. A thorough investigation of cell types transfected in animal models was not conducted. Knowledge of cell tropism will provide additional insight into suitable therapeutic targets and potential indications. For example, in the lung, robust delivery to basal and/or club cells would allow for the treatment of cystic fibrosis,<sup>101</sup> while delivery and expression in T cells would enable the development of chimeric antigen receptor T cell therapies. Additionally, we did not examine the delivery of genome editing cargoes, which have the potential to revolutionize treatment for many devastating genetic diseases. We also did not extensively assess long-term expression kinetics for therapeutic pDNA cargoes. While we demonstrate here the expression of a reporter (pDNA-FLuc) for up to 1 year, we found that the kinetics of expressed FST were substantially different than those of a reporter, for example. A comprehensive understanding of the mechanisms regulating therapeutic gene expression will vastly improve treatment strategies moving forward.

### STAR★METHODS

Detailed methods are provided in the online version of this paper and include the following:

- KEY RESOURCES TABLE
- RESOURCE AVAILABILITY
  - Lead contact
  - Materials availability
  - Data and code availability
- EXPERIMENTAL MODEL AND STUDY PARTICIPANT DETAILS
  - Cell Lines
  - Mouse Studies
  - Non-Human Primate (NHP) Studies
- METHOD DETAILS
  - Materials
  - Purification of FAST Proteins
  - Western Blot

### Figure 7. Delivery of pDNA encoding follistatin using FAST-PLVs

- (A) FAST-PLVs were used to encapsulate pDNA-CMV-FST (+) or pDNA-GFP (−) and added to C2C12 cells. Western blot was conducted to examine the expression of FST as well as phosphorylation of Akt and mTOR. Numbers above phosphorylated bands represent fold increase relative to pDNA-GFP.
- (B) Media concentration of FST following FAST-PLV addition to C2C12 mouse myoblasts determined via ELISA.
- (C) Serum levels of FST following a single intravenous injection of C57BL/6 mice with FAST-PLVs encapsulating 10 mg/kg pDNA-TTR-FST determined via ELISA. Data are represented as mean ± standard deviation,  $n = 3$  biologically independent mice.
- (D) Change in body weight of mice (normalized to initial measurement) over a period of several months, following a single intravenous injection on day 0 with PBS or FAST-PLVs encapsulating 10 mg/kg pDNA-TTR-FST. Two-way ANOVA and Dunnett's multiple comparisons test.
- (E) Change in hindlimb grip strength of mice (normalized to initial measurement) over a period of several months, following a single intravenous injection on day 0 with PBS or FAST-PLVs encapsulating 10 mg/kg pDNA-TTR-FST. Two-way ANOVA and Dunnett's multiple comparisons test.
- (F) Gross dissection of mice 34 weeks after intravenous injection with PBS or FAST-PLVs encapsulating 10 mg/kg pDNA-TTR-FST.
- (G) GAS muscle weight 34 weeks after FST treatment. Unpaired t test.
- (H) Representative images of GAS muscles stained with WGA-488 and DAPI.
- (I) GAS cross-sectional muscle fiber area determined using MyoVision Software. Two-way ANOVA and Dunnett's multiple comparisons test.

\* $p < 0.05$ , \*\* $p < 0.01$ , \*\*\* $p < 0.001$ , \*\*\*\* $p < 0.0001$ .

See also Figure S11.

- Syncytia Formation and Inhibition
- Lipid Formulations
- Nucleic Acid Quantification
- FAST-PLV Construction
- In Vitro Transfection
- Confocal Microscopy
- Imaging Flow Cytometry and Endocytosis Inhibition
- PLVs Characteristics and Encapsulation Efficiency
- Atomic Force Microscopy
- Transmission Electron Microscopy
- Viability Assay with Alamar Blue
- Lactate Dehydrogenase (LDH) Cytotoxicity Assay
- Whole Body and Ex Vivo Bioluminescence
- Biodistribution of pDNA in excised tissues
- Meso Scale Discovery – Cytokine and Chemokine Quantification
- Anti-Drug Antibody Titer: Indirect electrochemiluminescence immunoassay (ECLIA) for p14endo15 and FLuc
- MicroVue Complement C3a C4d and SC5b-9 Enzyme Immunoassay
- Follistatin ELISA
- Human Erythropoietin (EPO) ELISA
- Histology: Immunofluorescence, In-situ hybridization, and H&E staining

### ● QUANTIFICATION AND STATISTICAL ANALYSIS

### SUPPLEMENTAL INFORMATION

Supplemental information can be found online at <https://doi.org/10.1016/j.cell.2024.07.023>.

### ACKNOWLEDGMENTS

This research was supported by an operating grant to J.D.L. from the Canadian Institutes of Health Research (CIHR), in partnership with the Institute of Aging: Research Nova Scotia, reference number VR1-172710. J.D.L. holds the Bird Dogs Chair in Translational Oncology funded by the Alberta Cancer Foundation. R.D.'s laboratory was funded by the CIHR and the Natural Sciences and Engineering Research Council of Canada (NSERC). D.W.B. was funded by fellowships from Prostate Cancer Canada and Mitacs. E.K.C. was funded by scholarships from the Nova Scotia Health Research Foundation (NSHRF) and the Cancer Research Training Program (CRTP) and also received funding from the Dalhousie Medical Research Foundation (DMRF). We thank Abul Kalam Azad for isolating and sub-culturing HUVEC and Katia Carmine-Simmen for her technical support.

### AUTHOR CONTRIBUTIONS

Conceptualization, D.W.B., P.W., P.B., A.R., and J.D.L.; methodology, D.W.B., P.W., P.B., A.R., D.P., E.K.C., and J.D.L.; formal analysis, D.W.B., P.W., P.B.,

A.R., R.D., and E.K.C.; investigation, D.W.B., P.W., P.B., A.B., M.H., H.V., L.G., D.S., J.A., E.K.C., S.L., J.K., M.P.S.A., R.Q., F.E., N.R., N.G., B.T., A.D., S.G., N.M., M.P., J.G., H.G., and J.A.; visualization, D.W.B. and J.A.; writing—original draft, D.W.B. and P.H.B.; writing—review & editing, D.W.B., P.H.B., R.D., J.A., A.R., and J.D.L.; funding acquisition, M.S., R.D., and J.D.L.; supervision, A.R., D.M., M.S., R.D., and J.D.L.

#### DECLARATION OF INTERESTS

D.W.B., P.W., P.B., A.B., L.G., M.H., H.V., D.S., J.A., J.K., M.P.S.A., R.Q., B.R., F.E., N.R., L.M., N.G., B.T., A.D., M.P., J.G., C.M., P.H.B., A.R., R.D., and J.D.L. are employees and/or shareholders of Entos Pharmaceuticals. H.G., M.S., and J.D.L. are employees and/or shareholders of Oisin Biotechnologies. J.A., M.S., and J.D.L. are employees and/or shareholders of OncoSenX. E.K.C., D.P., M.S., A.R., R.D., and J.D.L. are authors on a patent related to this work.

Received: September 27, 2022

Revised: May 8, 2024

Accepted: July 12, 2024

Published: September 10, 2024

#### REFERENCES

1. Roberts, T.C., Langer, R., and Wood, M.J.A. (2020). Advances in oligonucleotide drug delivery. *Nat. Rev. Drug Discov.* 19, 673–694. <https://doi.org/10.1038/s41573-020-0075-7>.
2. He, X., Urip, B.A., Zhang, Z., Ngan, C.C., and Feng, B. (2021). Evolving AAV-delivered therapeutics towards ultimate cures. *J. Mol. Med. (Berl)* 99, 593–617. <https://doi.org/10.1007/s00109-020-02034-2>.
3. Thomas, C.E., Ehrhardt, A., and Kay, M.A. (2003). Progress and problems with the use of viral vectors for gene therapy. *Nat. Rev. Genet.* 4, 346–358. <https://doi.org/10.1038/nrg1066>.
4. Ginn, S.L., Amaya, A.K., Alexander, I.E., Edelstein, M., and Abedi, M.R. (2018). Gene therapy clinical trials worldwide to 2017: an update. *J. Gene Med.* 20, e3015. <https://doi.org/10.1002/jgm.3015>.
5. Bessis, N., GarciaCozar, F.J., and Boissier, M.C. (2004). Immune responses to gene therapy vectors: influence on vector function and effector mechanisms. *Gene Ther.* 11, S10–S17. <https://doi.org/10.1038/sj.gt.3302364>.
6. Halbert, C.L., Rutledge, E.A., Allen, J.M., Russell, D.W., and Miller, A.D. (2000). Repeat transduction in the mouse lung by using adeno-associated virus vectors with different serotypes. *J. Virol.* 74, 1524–1532. <https://doi.org/10.1128/jvi.74.3.1524-1532.2000>.
7. Boutin, S., Monteilhet, V., Veron, P., Leborgne, C., Benveniste, O., Montus, M.F., and Masurier, C. (2010). Prevalence of serum IgG and neutralizing factors against adeno-associated virus (AAV) types 1, 2, 5, 6, 8, and 9 in the healthy population: implications for gene therapy using AAV vectors. *Hum. Gene Ther.* 21, 704–712. <https://doi.org/10.1089/hum.2009.182>.
8. Nayak, S., and Herzog, R.W. (2010). Progress and prospects: immune responses to viral vectors. *Gene Ther.* 17, 295–304. <https://doi.org/10.1038/gt.2009.148>.
9. Masat, E., Pavani, G., and Mingozzi, F. (2013). Humoral immunity to AAV vectors in gene therapy: challenges and potential solutions. *Discov. Med.* 15, 379–389.
10. Ferreira, V., Twisk, J., Kwikkers, K., Aronica, E., Brisson, D., Methot, J., Petry, H., and Gaudet, D. (2014). Immune responses to intramuscular administration of alipogene tiparvovec (AAV1-LPL(S447X)) in a phase II clinical trial of lipoprotein lipase deficiency gene therapy. *Hum. Gene Ther.* 25, 180–188. <https://doi.org/10.1089/hum.2013.169>.
11. Jayaraman, M., Ansell, S.M., Mui, B.L., Tam, Y.K., Chen, J., Du, X., Butler, D., Eltepu, L., Matsuda, S., Narayananair, J.K., et al. (2012). Maximizing the potency of siRNA lipid nanoparticles for hepatic gene silencing *in vivo*. *Angew. Chem. Int. Ed. Engl.* 51, 8529–8533. <https://doi.org/10.1002/anie.201203263>.
12. György, B., Szabó, T.G., Pásztói, M., Pál, Z., Misják, P., Aradi, B., László, V., Pállinger, E., Pap, E., Kittel, A., et al. (2011). Membrane vesicles, current state-of-the-art: emerging role of extracellular vesicles. *Cell. Mol. Life Sci.* 68, 2667–2688. <https://doi.org/10.1007/s00018-011-0689-3>.
13. Kauffman, K.J., Dorkin, J.R., Yang, J.H., Heartlein, M.W., DeRosa, F., Mir, F.F., Fenton, O.S., and Anderson, D.G. (2015). Optimization of lipid nanoparticle formulations for mRNA delivery *in vivo* with fractional factorial and definitive screening designs. *Nano Lett.* 15, 7300–7306. <https://doi.org/10.1021/acs.nanolett.5b02497>.
14. Semple, S.C., Akinc, A., Chen, J., Sandhu, A.P., Mui, B.L., Cho, C.K., Sah, D.W.Y., Stebbing, D., Crosley, E.J., Yaworski, E., et al. (2010). Rational design of cationic lipids for siRNA delivery. *Nat. Biotechnol.* 28, 172–176. <https://doi.org/10.1038/nbt.1602>.
15. Gu, F., Zhang, L., Teply, B.A., Mann, N., Wang, A., Radovic-Moreno, A.F., Langer, R., and Farokhzad, O.C. (2008). Precise engineering of targeted nanoparticles by using self-assembled biointegrated block copolymers. *Proc. Natl. Acad. Sci. USA* 105, 2586–2591. <https://doi.org/10.1073/pnas.0711714105>.
16. Akinc, A., Zumbuehl, A., Goldberg, M., Leshchiner, E.S., Busini, V., Hosseini, N., Bacallado, S.A., Nguyen, D.N., Fuller, J., Alvarez, R., et al. (2008). A combinatorial library of lipid-like materials for delivery of RNAi therapeutics. *Nat. Biotechnol.* 26, 561–569. <https://doi.org/10.1038/nbt1402>.
17. Sabnis, S., Kumarasinghe, E.S., Salerno, T., Mihai, C., Ketova, T., Senn, J.J., Lynn, A., Bulychev, A., McFadyen, I., Chan, J., et al. (2018). A novel amino lipid series for mRNA delivery: improved endosomal escape and sustained pharmacology and safety in non-human primates. *Mol. Ther.* 26, 1509–1519. <https://doi.org/10.1016/j.ymthe.2018.03.010>.
18. Leslie, S.W., Soon-Sutton, T.L., and Siref, L.E. (2019). Prostate Cancer. In *StatPearls* (StatPearls Publishing).
19. Akinc, A., Maier, M.A., Manoharan, M., Fitzgerald, K., Jayaraman, M., Barros, S., Ansell, S., Du, X., Hope, M.J., Madden, T.D., et al. (2019). The Onpattro story and the clinical translation of nanomedicines containing nucleic acid-based drugs. *Nat. Nanotechnol.* 14, 1084–1087. <https://doi.org/10.1038/s41565-019-0591-y>.
20. Wan, C., Allen, T.M., and Cullis, P.R. (2014). Lipid nanoparticle delivery systems for siRNA-based therapeutics. *Drug Deliv. Transl. Res.* 4, 74–83. <https://doi.org/10.1007/s13346-013-0161-z>.
21. Cullis, P.R., and Hope, M.J. (2017). Lipid nanoparticle systems for enabling gene therapies. *Mol. Ther.* 25, 1467–1475. <https://doi.org/10.1016/j.ymthe.2017.03.013>.
22. Reichmuth, A.M., Oberli, M.A., Jaklenec, A., Langer, R., and Blankschtein, D. (2016). mRNA vaccine delivery using lipid nanoparticles. *Ther. Deliv.* 7, 319–334. <https://doi.org/10.4155/tde-2016-0006>.
23. Kulkarni, J.A., Cullis, P.R., and Van Der Meel, R. (2018). Lipid nanoparticles enabling gene therapies: from concepts to clinical utility. *Nucleic Acid Ther.* 28, 146–157. <https://doi.org/10.1089/nat.2018.0721>.
24. Hassett, K.J., Benenato, K.E., Jacquinot, E., Lee, A., Woods, A., Yuzhakov, O., Himansu, S., Deterling, J., Geilich, B.M., Ketova, T., et al. (2019). Optimization of lipid nanoparticles for intramuscular administration of mRNA vaccines. *Mol. Ther. Nucleic Acids* 15, 1–11. <https://doi.org/10.1016/j.omtn.2019.01.013>.
25. Xue, H.Y., Liu, S., and Wong, H.L. (2014). Nanotoxicity: a key obstacle to clinical translation of siRNA-based nanomedicine. *Nanomedicine (London, England)* 9, 295–312. <https://doi.org/10.2217/nnm.13.204>.
26. Sedic, M., Senn, J.J., Lynn, A., Laska, M., Smith, M., Platz, S.J., Bolen, J., Hoge, S., Bulychev, A., Jacquinot, E., et al. (2018). Safety evaluation of lipid nanoparticle-formulated modified mRNA in the Sprague-Dawley rat and cynomolgus monkey. *Vet. Pathol.* 55, 341–354. <https://doi.org/10.1177/0300985817738095>.

27. Ciechonska, M., and Duncan, R. (2014). Reovirus FAST proteins: virus-encoded cellular fusogens. *Trends Microbiol.* 22, 715–724. <https://doi.org/10.1016/j.tim.2014.08.005>.
28. Duncan, R. (2019). Fusogenic Reoviruses and their fusion-associated small transmembrane (FAST) proteins. *Annu. Rev. Virol.* 6, 341–363. <https://doi.org/10.1146/annurev-virology-092818-015523>.
29. Top, D., de Antueno, R., Salsman, J., Corcoran, J., Mader, J., Hoskin, D., Touhami, A., Jericho, M.H., and Duncan, R. (2005). Liposome reconstitution of a minimal protein-mediated membrane fusion machine. *EMBO J.* 24, 2980–2988. <https://doi.org/10.1038/sj.emboj.7600767>.
30. Dawe, S., Corcoran, J.A., Clancy, E.K., Salsman, J., and Duncan, R. (2005). Unusual topological arrangement of structural motifs in the baboon reovirus fusion-associated small transmembrane protein. *J. Virol.* 79, 6216–6226. <https://doi.org/10.1128/JVI.79.10.6216-6226.2005>.
31. Corcoran, J.A., and Duncan, R. (2004). Reptilian reovirus utilizes a small Type III protein with an external myristylated amino terminus to mediate cell-cell fusion. *J. Virol.* 78, 4342–4351. <https://doi.org/10.1128/JVI.78.4342-4351.2004>.
32. Salsman, J., Top, D., Boutilier, J., and Duncan, R. (2005). Extensive syncytium formation mediated by the reovirus FAST proteins triggers apoptosis-induced membrane instability. *J. Virol.* 79, 8090–8100. <https://doi.org/10.1128/JVI.79.13.8090-8100.2005>.
33. Top, D., Read, J.A., Dawe, S.J., Syvitski, R.T., and Duncan, R. (2012). Cell-cell membrane fusion induced by p15 fusion-associated small transmembrane (FAST) protein requires a novel fusion peptide motif containing a myristoylated proline-rich type II helix. *J. Biol. Chem.* 287, 3403–3414. <https://doi.org/10.1074/jbc.M111.305268>.
34. Parmar, H.B., Barry, C., and Duncan, R. (2014). Polybasic trafficking signal mediates Golgi export, ER retention or ER export and retrieval based on membrane-proximity. *PLoS One* 9, e94194. <https://doi.org/10.1371/journal.pone.0094194>.
35. Read, J., Clancy, E.K., Sarker, M., de Antueno, R., Langelaan, D.N., Parmar, H.B., Shin, K., Rainey, J.K., and Duncan, R. (2015). Reovirus FAST proteins drive pore formation and Syncytogenesis using a novel helix-loop-helix fusion-inducing lipid packing sensor. *PLOS Pathog.* 11, e1004962. <https://doi.org/10.1371/journal.ppat.1004962>.
36. Clancy, E.K., and Duncan, R. (2011). Helix-destabilizing, beta-branched, and polar residues in the baboon reovirus p15 transmembrane domain influence the modularity of FAST proteins. *J. Virol.* 85, 4707–4719. <https://doi.org/10.1128/JVI.02223-10>.
37. Clancy, E.K., and Duncan, R. (2009). Reovirus FAST protein transmembrane domains function in a modular, primary sequence-independent manner to mediate cell-cell membrane fusion. *J. Virol.* 83, 2941–2950. <https://doi.org/10.1128/JVI.01869-08>.
38. Richardson, A., de Antueno, R., Duncan, R., and Hoskin, D.W. (2009). Intracellular delivery of bovine lactoferricin's antimicrobial core (RRWQWR) kills T-leukemia cells. *Biochem. Biophys. Res. Commun.* 388, 736–741. <https://doi.org/10.1016/j.bbrc.2009.08.083>.
39. Yin, H., Kanasty, R.L., Eltoukhy, A.A., Vegas, A.J., Dorkin, J.R., and Anderson, D.G. (2014). Non-viral vectors for gene-based therapy. *Nat. Rev. Genet.* 15, 541–555. <https://doi.org/10.1038/nrg3763>.
40. Belliveau, N.M., Huff, J., Lin, P.J., Chen, S., Leung, A.K., Leaver, T.J., Wild, A.W., Lee, J.B., Taylor, R.J., Tam, Y.K., et al. (2012). Microfluidic synthesis of highly potent limit-size lipid nanoparticles for *in vivo* delivery of siRNA. *Mol. Ther. Nucleic Acids* 1, e37. <https://doi.org/10.1038/mtna.2012.28>.
41. Leung, A.K.K., Tam, Y.Y.C., Chen, S., Hafez, I.M., and Cullis, P.R. (2015). Microfluidic mixing: A general method for encapsulating macromolecules in lipid nanoparticle systems. *J. Phys. Chem. B* 119, 8698–8706. <https://doi.org/10.1021/acs.jpcb.5b02891>.
42. Chen, D., Love, K.T., Chen, Y., Eltoukhy, A.A., Kastrup, C., Sahay, G., Jeon, A., Dong, Y., Whitehead, K.A., and Anderson, D.G. (2012). Rapid discovery of potent siRNA-containing lipid nanoparticles enabled by controlled microfluidic formulation. *J. Am. Chem. Soc.* 134, 6948–6951. <https://doi.org/10.1021/ja301621z>.
43. Zerial, M., and McBride, H. (2001). Rab proteins as membrane organizers. *Nat. Rev. Mol. Cell Biol.* 2, 107–117. <https://doi.org/10.1038/35052055>.
44. Gilleron, J., Querbes, W., Zeigerer, A., Borodovsky, A., Marsico, G., Schubert, U., Manygoats, K., Seifert, S., Andree, C., Stöter, M., et al. (2013). Image-based analysis of lipid nanoparticle-mediated siRNA delivery, intracellular trafficking and endosomal escape. *Nat. Biotechnol.* 31, 638–646. <https://doi.org/10.1038/nbt.2612>.
45. Gorvel, J.P., Chavrier, P., Zerial, M., and Gruenberg, J. (1991). rab5 controls early endosome fusion *in vitro*. *Cell* 64, 915–925. [https://doi.org/10.1016/0092-8674\(91\)90316-q](https://doi.org/10.1016/0092-8674(91)90316-q).
46. Kirchhausen, T., Macia, E., and Pelish, H.E. (2008). Use of dynasore, the small molecule inhibitor of dynamin, in the regulation of endocytosis. *Methods Enzymol.* 438, 77–93. [https://doi.org/10.1016/S0076-6879\(07\)38006-3](https://doi.org/10.1016/S0076-6879(07)38006-3).
47. Preta, G., Cronin, J.G., and Sheldon, I.M. (2015). Dynasore - not just a dynamin inhibitor. *Cell Commun. Signal.* 13, 24. <https://doi.org/10.1186/s12964-015-0102-1>.
48. Sorkin, A., and Goh, L.K. (2008). Endocytosis and intracellular trafficking of ErBBS. *Exp. Cell Res.* 314, 3093–3106. <https://doi.org/10.1016/j.yexcr.2008.08.013>.
49. Wee, P., and Wang, Z. (2018). Regulation of EGFR endocytosis by CBL during mitosis. *Cells* 7, 257. <https://doi.org/10.3390/cells7120257>.
50. Omerovic, J., Hammond, D.E., Prior, I.A., and Clague, M.J. (2012). Global snapshot of the influence of endocytosis upon EGF receptor signaling output. *J. Proteome Res.* 11, 5157–5166. <https://doi.org/10.1021/pr3007304>.
51. Ablasser, A., Goldeck, M., Cavlar, T., Deimling, T., Witte, G., Röhl, I., Hopfner, K.P., Ludwig, J., and Hornung, V. (2013). cGAS produces a 2'-5'-linked cyclic dinucleotide second messenger that activates STING. *Nature* 498, 380–384. <https://doi.org/10.1038/nature12306>.
52. Ishikawa, H., Ma, Z., and Barber, G.N. (2009). STING regulates intracellular DNA-mediated, type I interferon-dependent innate immunity. *Nature* 461, 788–792. <https://doi.org/10.1038/nature08476>.
53. Diner, E.J., Burdette, D.L., Wilson, S.C., Monroe, K.M., Kellenberger, C.A., Hyodo, M., Hayakawa, Y., Hammond, M.C., and Vance, R.E. (2013). The innate immune DNA sensor cGAS produces a noncanonical cyclic dinucleotide that activates human STING. *Cell Rep.* 3, 1355–1361. <https://doi.org/10.1016/j.celrep.2013.05.009>.
54. Cardarelli, F., Di Giacomo, L., Marchini, C., Amici, A., Salomone, F., Fiume, G., Rossetta, A., Gratton, E., Pozzi, D., and Caracciolo, G. (2016). The intracellular trafficking mechanism of Lipofectamine-based transfection reagents and its implication for gene delivery. *Sci. Rep.* 6, 25879. <https://doi.org/10.1038/srep25879>.
55. Lv, H., Zhang, S., Wang, B., Cui, S., and Yan, J. (2006). Toxicity of cationic lipids and cationic polymers in gene delivery. *J. Control. Release* 114, 100–109. <https://doi.org/10.1016/j.jconrel.2006.04.014>.
56. Goswami, R., Subramanian, G., Silayeva, L., Newkirk, I., Doctor, D., Chawla, K., Chattopadhyay, S., Chandra, D., Chilukuri, N., and Betapudi, V. (2019). Gene therapy leaves a vicious cycle. *Front. Oncol.* 9, 297. <https://doi.org/10.3389/fonc.2019.00297>.
57. Elsabahy, M., and Wooley, K.L. (2013). Cytokines as biomarkers of nanoparticle immunotoxicity. *Chem. Soc. Rev.* 42, 5552–5576. <https://doi.org/10.1039/c3cs60064e>.
58. Arteta, M.Y., Kjellman, T., Bartesaghi, S., Wallin, S., Wu, X., Kvist, A.J., Dabkowska, A., Székely, N., Radulescu, A., and Bergenholz, J. (2018). Successful reprogramming of cellular protein production through mRNA delivered by functionalized lipid nanoparticles. *Proc. Natl. Acad. Sci. USA* 115, E3351–E3360.

59. Lowenstein, L.J. (2003). A primer of primate pathology: lesions and nonlesions. *Toxicol. Pathol.* 31, 92–102. <https://doi.org/10.1080/01926230390177668>.
60. Ward, K.W., Coon, D.J., Magiera, D., Bhadresa, S., Nisbett, E., and Lawrence, M.S. (2008). Exploration of the African green monkey as a preclinical pharmacokinetic model: intravenous pharmacokinetic parameters. *Drug Metab. Dispos.* 36, 715–720. <https://doi.org/10.1124/dmd.107.019315>.
61. Szelenyi, J. (2014). Complement activation-related pseudoallergy: A stress reaction in blood triggered by nanomedicines and biologicals. *Mol. Immunol.* 61, 163–173. <https://doi.org/10.1016/j.molimm.2014.06.038>.
62. Szelenyi, J., Bedőcs, P., Rozsnay, Z., Weiszár, Z., Urbanics, R., Rosivall, L., Cohen, R., Garbuzenko, O., Báthori, G., Tóth, M., et al. (2012). Liposome-induced complement activation and related cardiopulmonary distress in pigs: factors promoting reactogenicity of Doxil and AmBisome. *Nanomedicine* 8, 176–184. <https://doi.org/10.1016/j.nano.2011.06.003>.
63. Lee, S.J., and McPherron, A.C. (2001). Regulation of myostatin activity and muscle growth. *Proc. Natl. Acad. Sci. USA* 98, 9306–9311. <https://doi.org/10.1073/pnas.151270098>.
64. Mendell, J.R., Al-Zaidy, S., Shell, R., Arnold, W.D., Rodino-Klapac, L.R., Prior, T.W., Lowes, L., Alfano, L., Berry, K., Church, K., et al. (2017). Single-dose gene-replacement therapy for spinal muscular atrophy. *N. Engl. J. Med.* 377, 1713–1722. <https://doi.org/10.1056/NEJMoa1706198>.
65. Al-Zaidy, S.A., Sahenk, Z., Rodino-Klapac, L.R., Kaspar, B., and Mendell, J.R. (2015). Follistatin gene therapy improves ambulation in Becker muscular dystrophy. *J. Neuromuscul. Dis.* 2, 185–192. <https://doi.org/10.3233/JND-150083>.
66. Winbanks, C.E., Weeks, K.L., Thomson, R.E., Sepulveda, P.V., Beyer, C., Qian, H., Chen, J.L., Allen, J.M., Lancaster, G.I., Febbraio, M.A., et al. (2012). Follistatin-mediated skeletal muscle hypertrophy is regulated by Smad3 and mTOR independently of myostatin. *J. Cell Biol.* 197, 997–1008. <https://doi.org/10.1083/jcb.201109091>.
67. Hansen, J.S., Rutti, S., Arous, C., Clemmesen, J.O., Secher, N.H., Drescher, A., Gonelle-Gispert, C., Halban, P.A., Pedersen, B.K., Weigert, C., et al. (2016). Circulating follistatin is liver-derived and regulated by the glucagon-to-insulin ratio. *J. Clin. Endocrinol. Metab.* 101, 550–560. <https://doi.org/10.1210/jc.2015-3668>.
68. Corcoran, J.A., Syvitski, R., Top, D., Epand, R.M., Epand, R.F., Jakeman, D., and Duncan, R. (2004). Myristoylation, a protruding loop, and structural plasticity are essential features of a nonenveloped virus fusion peptide motif. *J. Biol. Chem.* 279, 51386–51394. <https://doi.org/10.1074/jbc.M406990200>.
69. Fitzgerald, K., White, S., Borodovsky, A., Bettencourt, B.R., Strahs, A., Clausen, V., Wijngaard, P., Horton, J.D., Taubel, J., Brooks, A., et al. (2017). A highly durable RNAi therapeutic inhibitor of PCSK9. *N. Engl. J. Med.* 376, 41–51. <https://doi.org/10.1056/NEJMoa1609243>.
70. Paunovska, K., Gil, C.J., Lokugamage, M.P., Sago, C.D., Sato, M., Lando, G.N., Gamboa Castro, M., Bryksin, A.V., and Dahlman, J.E. (2018). Analyzing 2000 *in vivo* drug delivery data points reveals cholesterol structure impacts nanoparticle delivery. *ACS Nano* 12, 8341–8349. <https://doi.org/10.1021/acsnano.8b03640>.
71. Nathwani, A.C., Reiss, U.M., Tuddenham, E.G.D., Rosales, C., Chowdary, P., McIntosh, J., Della Peruta, M., Lheriteau, E., Patel, N., Raj, D., et al. (2014). Long-term safety and efficacy of factor IX gene therapy in hemophilia B. *N. Engl. J. Med.* 371, 1994–2004. <https://doi.org/10.1056/NEJMoa1407309>.
72. Keeler, A.M., and Flotte, T.R. (2019). Recombinant adeno-associated virus gene therapy in light of Luxturna (and Zolgensma and Glybera): where are we, and how did we get here? *Annu. Rev. Virol.* 6, 601–621. <https://doi.org/10.1146/annurev-virology-092818-015530>.
73. Flotte, T.R., Schwiebert, E.M., Zeitlin, P.L., Carter, B.J., and Guggino, W.B. (2005). Correlation between DNA transfer and cystic fibrosis airway epithelial cell correction after recombinant adeno-associated virus serotype 2 gene therapy. *Hum. Gene Ther.* 16, 921–928. <https://doi.org/10.1089/hum.2005.16.921>.
74. Flotte, T.R., Zeitlin, P.L., Reynolds, T.C., Heald, A.E., Pedersen, P., Beck, S., Conrad, C.K., Brass-Ernst, L., Humphries, M., Sullivan, K., et al. (2003). Phase I trial of intranasal and endobronchial administration of a recombinant adeno-associated virus Serotype 2 (rAAV2)-CFTR vector in adult cystic fibrosis patients: A two-part clinical study. *Hum. Gene Ther.* 14, 1079–1088. <https://doi.org/10.1089/104303403322124792>.
75. Manno, C.S., Pierce, G.F., Arruda, V.R., Glader, B., Ragni, M., Rasko, J.J.E., Ozelo, M.C., Hoots, K., Blatt, P., Konkle, B., et al. (2006). Successful transduction of liver in hemophilia by AAV-factor IX and limitations imposed by the host immune response. *Nat. Med.* 12, 342–347. <https://doi.org/10.1038/nm1358>.
76. Mingozzi, F., Meulenbergh, J.J., Hui, D.J., Basner-Tschakarjan, E., Hasbrouck, N.C., Edmonson, S.A., Hutnick, N.A., Betts, M.R., Kastelein, J.J., Stroes, E.S., et al. (2009). AAV-1-mediated gene transfer to skeletal muscle in humans results in dose-dependent activation of capsid-specific T cells. *Blood* 114, 2077–2086. <https://doi.org/10.1182/blood-2008-07-167510>.
77. Mendell, J.R., Sahenk, Z., Al-Zaidy, S., Rodino-Klapac, L.R., Lowes, L.P., Alfano, L.N., Berry, K., Miller, N., Yalvac, M., Dvorchik, I., et al. (2017). Follistatin gene therapy for sporadic inclusion body myositis improves functional outcomes. *Mol. Ther.* 25, 870–879. <https://doi.org/10.1016/j.ymthe.2017.02.015>.
78. Kota, J., Handy, C.R., Haidet, A.M., Montgomery, C.L., Eagle, A., Rodino-Klapac, L.R., Tucker, D., Shilling, C.J., Therifall, W.R., Walker, C.M., et al. (2009). Follistatin gene delivery enhances muscle growth and strength in nonhuman primates. *Sci. Transl. Med.* 1, 6ra15. <https://doi.org/10.1126/scitranslmed.3000112>.
79. Haidet, A.M., Rizo, L., Handy, C., Umapathi, P., Eagle, A., Shilling, C., Boue, D., Martin, P.T., Sahenk, Z., Mendell, J.R., et al. (2008). Long-term enhancement of skeletal muscle mass and strength by single gene administration of myostatin inhibitors. *Proc. Natl. Acad. Sci. USA* 105, 4318–4322. <https://doi.org/10.1073/pnas.0709144105>.
80. Mendell, J.R., Sahenk, Z., Malik, V., Gomez, A.M., Flanigan, K.M., Lowes, L.P., Alfano, L.N., Berry, K., Meadows, E., Lewis, S., et al. (2015). A phase 1/2a follistatin gene therapy trial for Becker muscular dystrophy. *Mol. Ther.* 23, 192–201. <https://doi.org/10.1038/mt.2014.200>.
81. Wang, D., Tai, P.W.L., and Gao, G. (2019). Adeno-associated virus vector as a platform for gene therapy delivery. *Nat. Rev. Drug Discov.* 18, 358–378. <https://doi.org/10.1038/s41573-019-0012-9>.
82. Chew, W.L., Tabebordbar, M., Cheng, J.K.W., Mali, P., Wu, E.Y., Ng, A.H.M., Zhu, K., Wagers, A.J., and Church, G.M. (2016). A multifunctional AAV-CRISPR-Cas9 and its host response. *Nat. Methods* 13, 868–874. <https://doi.org/10.1038/nmeth.3993>.
83. Mali, P., Yang, L., Esvelt, K.M., Aach, J., Guell, M., DiCarlo, J.E., Norville, J.E., and Church, G.M. (2013). RNA-guided human genome engineering via Cas9. *Science* 339, 823–826. <https://doi.org/10.1126/science.1232033>.
84. Sander, J.D., and Joung, J.K. (2014). CRISPR-Cas systems for editing, regulating and targeting genomes. *Nat. Biotechnol.* 32, 347–355. <https://doi.org/10.1038/nbt.2842>.
85. Colella, P., Ronzitti, G., and Mingozzi, F. (2018). Emerging issues in AAV-mediated *in vivo* gene therapy. *Mol. Ther. Methods Clin. Dev.* 8, 87–104. <https://doi.org/10.1016/j.omtm.2017.11.007>.
86. Baden, L.R., El Sahly, H.M., Essink, B., Kotloff, K., Frey, S., Novak, R., Diemert, D., Spector, S.A., Roush, N., Creech, C.B., et al. (2021). Efficacy and safety of the mRNA-1273 SARS-CoV-2 vaccine. *N. Engl. J. Med.* 384, 403–416. <https://doi.org/10.1056/NEJMoa2035389>.
87. Wu, K., Choi, A., Koch, M., Ma, L., Hill, A., Nunna, N., Huang, W., Oestreicher, J., Colpitts, T., Bennett, H., et al. (2021). Preliminary analysis of safety and immunogenicity of a SARS-CoV-2 variant vaccine booster. Preprint at medRxiv. <https://doi.org/10.1101/2021.05.05.21256716>.

88. Sahin, U., Muik, A., Derhovanessian, E., Vogler, I., Kranz, L.M., Vormehr, M., Baum, A., Pascal, K., Quandt, J., Maurus, D., et al. (2020). COVID-19 vaccine BNT162b1 elicits human antibody and TH1 T cell responses. *Nature* 586, 594–599. <https://doi.org/10.1038/s41586-020-2814-7>.
89. Corbett, K.S., Edwards, D.K., Leist, S.R., Abiona, O.M., Boyoglu-Barnum, S., Gillespie, R.A., Himansu, S., Schäfer, A., Ziawo, C.T., Di-Piazza, A.T., et al. (2020). SARS-CoV-2 mRNA vaccine design enabled by prototype pathogen preparedness. *Nature* 586, 567–571. <https://doi.org/10.1038/s41586-020-2622-0>.
90. Anderson, E.J., Roush, N.G., Widge, A.T., Jackson, L.A., Roberts, P.C., Makhene, M., Chappell, J.D., Denison, M.R., Stevens, L.J., Pruijssers, A.J., et al. (2020). Safety and immunogenicity of SARS-CoV-2 mRNA-1273 vaccine in older adults. *N. Engl. J. Med.* 383, 2427–2438. <https://doi.org/10.1056/NEJMoa2028436>.
91. Jorritsma, S.H.T., Gowans, E.J., Grubor-Bauk, B., and Wijesundara, D.K. (2016). Delivery methods to increase cellular uptake and immunogenicity of DNA vaccines. *Vaccine* 34, 5488–5494. <https://doi.org/10.1016/j.vaccine.2016.09.062>.
92. Hannaman, D., Dupuy, L.C., Ellefson, B., and Schmaljohn, C.S. (2016). A Phase 1 clinical trial of a DNA vaccine for Venezuelan equine encephalitis delivered by intramuscular or intradermal electroporation. *Vaccine* 34, 3607–3612. <https://doi.org/10.1016/j.vaccine.2016.04.077>.
93. Houser, K.V., Yamshchikov, G.V., Bellamy, A.R., May, J., Enama, M.E., Sarwar, U., Larkin, B., Bailer, R.T., Koup, R., Paskel, M., et al. (2018). DNA vaccine priming for seasonal influenza vaccine in children and adolescents 6 to 17 years of age: A phase 1 randomized clinical trial. *PLoS One* 13, e0206837. <https://doi.org/10.1371/journal.pone.0206837>.
94. Modjarrad, K., Roberts, C.C., Mills, K.T., Castellano, A.R., Paolino, K., Muthuman, K., Reuschel, E.L., Robb, M.L., Racine, T., Oh, M.-D., et al. (2019). Safety and immunogenicity of an anti-Middle East respiratory syndrome coronavirus DNA vaccine: a phase 1, open-label, single-arm, dose-escalation trial. *Lancet Infect. Dis.* 19, 1013–1022. [https://doi.org/10.1016/S1473-3099\(19\)30266-X](https://doi.org/10.1016/S1473-3099(19)30266-X).
95. Tebas, P., Kraynyak, K.A., Patel, A., Maslow, J.N., Morrow, M.P., Sylvester, A.J., Knoblock, D., Gillespie, E., Amante, D., Racine, T., et al. (2019). Intradermal SynCon® Ebola GP DNA vaccine is temperature stable and safely demonstrates cellular and humoral immunogenicity advantages in healthy volunteers. *J. Infect. Dis.* 220, 400–410. <https://doi.org/10.1093/infdis/jiz132>.
96. Pardi, N., Hogan, M.J., Porter, F.W., and Weissman, D. (2018). mRNA vaccines — a new era in vaccinology. *Nat. Rev. Drug Discov.* 17, 261–279. <https://doi.org/10.1038/nrd.2017.243>.
97. Basu, A., and Chakraborty, S. (2017). Faculty Opinions Recommendation of Zika Virus Protection by a Single Low-Dose Nucleoside-Modified mRNA Vaccination. *Faculty Opinions – Post-publication Peer Review of the Biomedical Literature (Faculty Opinions Ltd.)*.
98. Raturi, A., Ablack, J., Wee, P., Bhandari, P., Brown, D., Hejazi, M., McMullen, N., Grin, L., Vega, H., Garcia, H., et al. (2022). Immunogenicity of SARS-CoV-2 DNA Vaccine Candidates Formulated with the Fusion-Associated Small Transmembrane Protein Proteolipid Vehicle Delivery System. [https://papers.ssm.com/sol3/papers.cfm?abstract\\_id=4241174](https://papers.ssm.com/sol3/papers.cfm?abstract_id=4241174).
99. Jackson, L.A., Anderson, E.J., Roush, N.G., Roberts, P.C., Makhene, M., Coler, R.N., McCullough, M.P., Chappell, J.D., Denison, M.R., Stevens, L.J., et al. (2020). An mRNA vaccine against SARS-CoV-2 — preliminary report. *N. Engl. J. Med.* 383, 1920–1931. <https://doi.org/10.1056/NEJMoa2022483>.
100. Roche, J.A., Ford-Speelman, D.L., Ru, L.W., Densmore, A.L., Roche, R., Reed, P.W., and Bloch, R.J. (2011). Physiological and histological changes in skeletal muscle following *in vivo* gene transfer by electroporation. *Am. J. Physiol. Cell Physiol.* 301, C1239–C1250. <https://doi.org/10.1152/ajpcell.00431.2010>.
101. Okuda, K., Dang, H., Kobayashi, Y., Carraro, G., Nakano, S., Chen, G., Kato, T., Asakura, T., Gilmore, R.C., Morton, L.C., et al. (2021). Secretory cells dominate airway CFTR expression and function in human airway superficial epithelia. *Am. J. Respir. Crit. Care Med.* 203, 1275–1289. <https://doi.org/10.1164/rccm.202008-3198OC>.
102. Schoenmaker, L., Witzigmann, D., Kulkarni, J.A., Verbeke, R., Kersten, G., Jiskoot, W., and Crommelin, D.J.A. (2021). mRNA-lipid nanoparticle COVID-19 vaccines: structure and stability. *Int. J. Pharm.* 601, 120586. <https://doi.org/10.1016/ijpharm.2021.120586>.
103. Hou, X., Zaks, T., Langer, R., and Dong, Y. (2021). Lipid nanoparticles for mRNA delivery. *Nat. Rev. Mater.* 6, 1078–1094. <https://doi.org/10.1038/s41578-021-00358-0>.
104. Oba, Y., Ojika, M., and Inouye, S. (2003). Firefly luciferase is a bifunctional enzyme: ATP-dependent monooxygenase and a long chain fatty acyl-CoA synthetase. *FEBS Lett.* 540, 251–254. [https://doi.org/10.1016/s0014-5793\(03\)00272-2](https://doi.org/10.1016/s0014-5793(03)00272-2).
105. IDEAS (2013). *Image Data Exploration and Analysis Software Users Manual, Sixth Edition (Amnis)*.
106. Wen, Y., Murach, K.A., Vechetti, I.J., Jr., Fry, C.S., Vickery, C., Peterson, C.A., McCarthy, J.J., and Campbell, K.S. (2018). MyoVision: software for automated high-content analysis of skeletal muscle immunohistochemistry. *J. Appl. Physiol.* (1985) 124, 40–51. <https://doi.org/10.1152/japplphysiol.00762.2017>.

## STAR★METHODS

### KEY RESOURCES TABLE

REAGENT or RESOURCE	SOURCE	IDENTIFIER
<b>Antibodies</b>		
Anti-GFP antibody	Abcam	Cat#ab13970; RRID:AB_300798
anti-GAPDH antibody	Abcam	Cat#ab8245; RRID:AB_2107448
Rabbit polyclonal p14endo15 antibody	New England Peptide	Produced in Study
Goat Anti-Human Follistatin Polyclonal antibody, Unconjugated	R&D systems	Cat#AF669; RRID:AB_2247223
Phospho-Akt Ser473	Cell Signaling Technology	Cat#4060; RRID:AB_2315049
Pan-Akt	Cell Signaling Technology	Cat#5239; RRID:AB_10544406
phospho-mTOR Ser2448	Cell Signaling Technology	Cat#2971; RRID:AB_330970
Anti-mTOR	Cell Signaling Technology	Cat#2972; RRID:AB_330978
Goat anti-Rabbit IgG (Heavy Chain), Superclonal Recombinant Secondary Antibody, Alexa Fluor 680	Thermo Fisher Scientific	Cat#A27042; RRID:AB_2536103
Donkey anti-goat Alexa Fluor 680	Thermo Fisher Scientific	Cat#A-21084; RRID:AB_2535741
goat anti-mouse Alexa Fluor 750	Thermo Fisher Scientific	Cat#A-21037; RRID:AB_2535708
sulfo-tag anti-mouse	Meso Scale Discovery	Cat#R32AC; RRID:AB_2783819
anti-NHP secondary antibody	Meso Scale Discovery	made by request
Goat anti-Chicken IgY (H+L) Secondary Antibody, Alexa Fluor 488	Thermo Fisher Scientific	Cat#A-11039; RRID:AB_2534096
<b>Chemicals, Peptides, and Recombinant Proteins</b>		
1,2-di-O-octadecenyl-3-trimethylammonium propane (DOTMA)	NOF Co.	Cat#CLE8181TA
1,2-dioleoyl-3-dimethylammonium-propane (DODAP)	NOF Co.	Cat#CL8181DA
1,2-dimyristoyl-sn-glycero-3-methoxypolyethylene glycol-2000 (DMG-PEG)	NOF Co.	Cat#GM020
2-dioleoyl-sn-glycero-3-phosphoethanolamine (DOPE)	Avanti Polar Lipids	Cat#850725P
1,2-dioleoyl-3-trimethylammonium-propane (DOTAP)	Avanti Polar Lipids	Cat#890890P
DLin-MC3-DMA (MC3)	Precision Bio Laboratories	made by request
Harris modified hematoxylin	Millipore Sigma	Cat#HHS32
Gill's hematoxylin I	Millipore Sigma	Cat#GHS132
Eosin Y	Millipore Sigma	Cat#318906
Resazurin sodium salt	Millipore Sigma	Cat#R7017
GFP Probe	Advanced Cell Diagnostics	Cat#538851
EGM-2 BulletKit	Lonza	Cat#CC-3162
Complete Hepatocyte Medium Kit	Cell Biologics	Cat#M1365
rat astrocyte growth medium	Cell Applications Inc.	Cat#R821-500
CellMask Deep Red	Thermo Scientific	Cat#C10046
CellMask Green	Thermo Scientific	Cat#C37608
Hoechst 33342	Thermo Scientific	Cat#H21492
Recombinant firefly luciferase protein	Novus Biologicals	Cat#NBP1-48355
ALC-0315	Avanti Polar Lipids	Cat#890900O
SM-102	Cayman Chemicals	Cat#33474
<b>Critical Commercial Assays</b>		
Lipofectamine 2000	Thermo Fisher Scientific	Cat#11668019
RNAScope Brown kit	Advanced Cell Diagnostics	Cat#322300
Universal 'Dip' Cell Kit	Malvern	Cat#ZEN1002
Quant-IT PicoGreen dsDNA assay	Thermo Fisher Scientific	Cat#P11496
DNeasy Blood & Tissue Kit	Qiagen	Cat#69504
QuickPlex SQ 120	Meso Scale Discovery	Cat#A11AA-0

(Continued on next page)

**Continued**

REAGENT or RESOURCE	SOURCE	IDENTIFIER
V-PLEX NHP cytokine 24-Plex Kit	Meso Scale Discovery	Cat#K15058D
V-PLEX Proinflammatory Panel 1 mouse kit	Meso Scale Discovery	Cat#K15048D
MicroVue complement C3a/C4d/SC5b-9 Plus EIA kits	Quidel	Cat#A032 XUS
human follistatin ELISA kit	PeproTech	Cat#900-K299
U-PLEX Human EPO Assay kit	Meso Scale Discovery	Cat#K151VXK-2
Bac to Bac Vector Kit	Thermofisher	10360014
CyQUANT LDH Cytotoxicity Assay	Thermo Fisher Scientific	Cat#C20300
<b>Experimental Models: Cell Lines</b>		
Quail fibrosarcoma (QM5) cells	Thermo Fisher Scientific	N/A
Human hepatocellular carcinoma cells (HEP3B)	ATCC	HB-8064
human non-small cell lung cancer cells	ATCC	NCI-H1299
human lung fibroblast cells IMR-90	ATCC	CCL-186
mouse embryo fibroblast cells (3T3)	ATCC	CRL-1658
VERO cells ( <i>Cercopithecus aethiops</i> epithelial kidney cells)	ATCC	CCL-81
mouse myoblasts (C2C12)	ATCC	CRL-1772
Human retinal pigmented epithelium cells (ARPE-19)	gift from Dr. Ian MacDonald (University of Alberta)	N/A
Human umbilical vein endothelial cells (HUVEC)	gift from Dr. Allan Murray (University of Alberta)	N/A
Sprague-Dawley Rat Primary Hepatocytes	Cell Biologics	Catalog No. RA-6224F
Primary rat astrocytes	Cell Applications Inc.	R882A-05n
human lung fibroblast cells WI-38	ATCC	CCL-75
Human Embryonic Kidney 293 T	ATCC	CRL-3216
Human Myocyte cells (AC10)	ATCC	CRL-3569
<b>Experimental Models: Organisms/Strains</b>		
Mouse: C57BL/6: H2 <sup>b</sup> , 027	Charles River Laboratories	N/A
African green monkeys ( <i>Chlorocebus sabaeus</i> )	Virscio, Inc	Wild type
<b>Software and Algorithms</b>		
Gwyddion software	<a href="http://gwyddion.net/">http://gwyddion.net/</a>	Free software
Molecular Imaging Software	Bruker	N/A
Living Image Software	Perkin Elmer	N/A
MyoVision software	<a href="http://www.MyoVision.org">www.MyoVision.org</a>	Free software
Image Data Exploration and Analysis Software (IDEAS)	Amnis	Imagestream Software

## RESOURCE AVAILABILITY

### Lead contact

Further information and requests for resources and reagents should be directed to and will be fulfilled by the lead contact, John D. Lewis ([jdlLewis@ualberta.ca](mailto:jdlLewis@ualberta.ca)).

### Materials availability

This study did not generate new unique reagents.

### Data and code availability

Section 1: All data reported in this paper will be shared by the [lead contact](#) upon request.

Section 2: This paper does not report original code.

Section 3: Any additional information required to reanalyze the data reported in this paper is available from the [lead contact](#) upon request.

## EXPERIMENTAL MODEL AND STUDY PARTICIPANT DETAILS

### Cell Lines

Quail fibrosarcoma (QM5) cells were cultured in Medium 199 with 3% fetal bovine serum (FBS; Sigma) and 0.5% penicillin/streptomycin (Thermo Fisher Scientific, Edmonton, Canada). Human hepatocellular carcinoma cells (HEP3B), human non-small cell lung cancer cells (NCI-H1299), human lung fibroblast cells (IMR-90 and WI-38), mouse embryo fibroblast cells (3T3), VERO CCL-81 cells (*Cercopithecus aethiops* epithelial kidney cells), and mouse myoblasts (C2C12) were purchased from ATCC (Manassas, VA) and cultured in high glucose-DMEM with 10% FBS and 1% penicillin/streptomycin. Human retinal pigmented epithelium cells (ARPE-19) were a gift from Dr. Ian MacDonald (University of Alberta) and were cultured in DMEM/F12 with 10% FBS and 1% penicillin/streptomycin. Benign prostatic hyperplasia cells (BPH-1) were purchased from Millipore Sigma and cultured in DMEM/F12 with 10% FBS and 1% penicillin/streptomycin. Human umbilical vein endothelial cells (HUVEC) were a gift from Dr. Allan Murray (University of Alberta) and were cultured in EGM-2 BulletKit (Lonza, Cat No. CC-3162). Sprague-Dawley Rat Primary Hepatocytes were purchased from Cell Biologics and were cultured in Complete Hepatocyte Medium Kit from Cell Biologics (Cat No. M1365). Primary rat astrocytes (Cat. No. R882A-05n) were cultured in rat astrocyte growth medium (Cat. No. R821-500, both purchased from Cell Applications Inc., San Diego, USA). Mammalian adherent cells were grown in tissue-culture treated 75 cm<sup>2</sup> flasks (VWR 10062-860) until cells were 80% confluent or nutrients in the media are depleted in a 37°C incubator with humidified atmosphere of 5% CO<sub>2</sub> (Nuaire NU-5510). *Spodoptera frugiperda* pupal ovarian tissue (Sf9) cells were stepwise cultured at 25°C to 2x10<sup>6</sup>–4x10<sup>6</sup> cells/mL from 25 mL to 100 mL and finally into a 2 L wave bioreactor. The Trypan Blue assay was used to check for cell viability.

### Mouse Studies

All animal studies were carried out according to the guidelines of the Canadian Council on Animal Care (CCAC) and approved by the University of Alberta Animal Care and Use Committee. *In vivo* studies were done using adult, 8–12-week-old, male and female C57BL/6 (Charles River Laboratories, Saint-Constant, Canada). Animals were group-housed in IVCs under SPF conditions, with constant temperature and humidity with lighting on a fixed light/dark cycle (12-hours/12-hours). Intravenous injection occurred via the lateral tail vein with 200 µL of the test agent. Intramuscular injection occurred in the gastrocnemius muscle of the hind limb with 50 µL of the test agent. These volume restrictions were used in part to select doses used for this study. Blood was collected via the lateral tail vein or cardiac puncture at indicated time points into serum collection tubes (Sarstedt, Montreal, Canada). Intrathecal injection was conducted by inserting a 31G needle into the L4-L5 intradural space and once a ‘tail flick’ response was observed, 10µL of test article was administered. Intracerebral ventricular injection was conducted using the coordinates –0.5 mm in the anteroposterior axis, +1 mm in the mediolateral axis and –2.3 mm in the dorsoventral axis. A 31G Hamilton syringe was inserted into the lateral ventricle of the right hemisphere and 5µL was dispensed at a rate of 1µL/minute before removing the needle at a rate of 0.5mm every 30 seconds to prevent leakage from the injection site. Intravitreal injection was conducted by inserting a 34G Hamilton syringe into the limbus of the eye and injecting 2µL of test article into the vitreous humor. Hindlimb grip strength was measured in quintuplicate using a T-bar attachment on the BIOSEB grip strength meter (Panlab, Cat. No. BSBI0GS3BS 76-1066).

### Non-Human Primate (NHP) Studies

All in-life NHP procedures were carried out by Virscio, Inc, under the guidance of the Institutional Animal Care and Use Committee (IACUC) of the St. Kitts Biomedical Research Foundation (SKBRF), St Kitts, West Indies. SKBRF research facility is fully accredited by the Association for Assessment and Accreditation of Laboratory Animal Care International (AAALAC International). African green monkeys (*Chlorocebus sabaeus*) are an invasive species on the island of St. Kitts and were procured locally using approved practices with IACUC oversight. Animals included in this study had estimated ages of 5–10 years, post breeding age, with an average estimated age of 8 years. The animals were housed in well-ventilated outdoor enclosures for the duration of the study. PLVs were infused into the saphenous or cephalic vein at a rate of 2 mL/min. Blood was collected via femoral or saphenous vein phlebotomy following overnight fasting under ketamine/xylazine anesthesia. Blood was transferred to Vacutainer serum collection tubes without clot activators (BD Medical, New Jersey, USA) for 1 hour at room temperature to allow clotting followed by centrifugation at 3000 rpm for 10 minutes at 4°C. At scheduled sacrifice, animals were sedated with ketamine and xylazine (8 mg/kg and 1.6 mg/kg respectively, IM) and euthanized with sodium pentobarbital (25–30 mg/kg IV). Upon loss of corneal reflex, transcardial perfusion was performed with chilled, heparinized 0.9% saline, and the brain and spinal cord were removed. Following perfusion, a gross necropsy was conducted. All abnormal findings were recorded, and associated tissues were collected and post-fixed in formalin for histopathology. Serum samples were sent to Antech Diagnostics (Los Angeles, CA) for clinical chemistry evaluation.

## METHOD DETAILS

### Materials

The following lipids were purchased from NOF Co. (Tokyo, Japan): 1,2-di-O-octadecenyl-3-trimethylammonium propane (DOTMA), 1,2-dioleoyl-3-dimethylammonium-propane (DODAP), 1,2-dimyristoyl-sn-glycero-3-methoxypolyethylene glycol-2000 (DMG-PEG), 2-dioleoyl-sn-glycero-3-phosphoethanolamine (DOPE) and 1,2-dioleoyl-3-trimethylammonium-propane (DOTAP) were purchased from Avanti Polar Lipids (Alabaster, USA). DLin-MC3-DMA (MC3) was purchased from Precision Bio Laboratories (Edmonton,

Canada). Plasmid DNA (pDNA) with the cytomegalovirus (CMV) promoter driving the DNA-encoded inserts, green fluorescent protein (GFP), and firefly luciferase (FLuc) was cloned into the Nanoplasmid vector produced by Nature Technology Company (Lincoln, USA). pDNA encoding the follistatin 344 splice variant under the transthyretin (TTR) and CMV promoters was also cloned into the Nano-plasmid produced by Nature Technology Company CleanCap mRNA with mRNA-encoded inserts; monomeric red fluorescent protein (mCherry), enhanced green fluorescent protein (eGFP), and firefly luciferase (FLuc) was purchased from TriLink Biotechnologies (San Diego, USA). siRNA targeting HPRT1 conjugated to Cy5 (siRNA-Cy5) was purchased from Horizon Discovery (Cambridge, United Kingdom). Lipofectamine 2000 and CyQUANT LDH Cytotoxicity Assay was purchased from Thermo Fisher Scientific (Edmonton, Canada). Harris modified hematoxylin and Gill's hematoxylin I was purchased from Fisher Scientific (Ottawa, Canada). Eosin Y and resazurin were purchased from Millipore Sigma (Oakville, Canada). RNAScope kit (Cat. No. 322300) and GFP probe (Cat. No. 538851) were purchased from Advanced Cell Diagnostics (Newark, USA). Anti-GFP antibody (ab13970) and anti-GAPDH antibody (ab8245) were purchased from Abcam (Cambridge, United Kingdom). Rabbit polyclonal p14endo15 antibody was produced by New England Peptide (Gardner, USA), using the target sequence Ac-PSNFVNHAPGEAIVTGLEKGADKVAGTC-Amide. Goat anti-follistatin antibody (AF669) was purchased from R&D systems (Minneapolis, USA). Phospho-Akt Ser473 (4069), pan-Akt (2920), phosphor-mTOR Ser2448 (2971), and mTOR (2972) antibodies were purchased from Cell Signaling Technology (Danvers, USA).

### Purification of FAST Proteins

P14endo15 was cloned into a pFastBac1 vector and used to generate a bacmid stock using the Bac-to-bac vector kit (Thermo Scientific, Cat. No. 10360014) following manufacturer's guidelines. Sf9 cells were transfected with the resulting bacmid and grown for 7 days until cell viability reached 70%. Sf9 cells are pelleted, and the supernatant is sterile filtered through a 0.8/0.2 μm filter to isolate baculovirus stock. Naïve Sf9 cells are infected with baculovirus stock and grown until cell viability reached 70%, following which the cells are pelleted and lysed with PBS + 1% n-Octyl-β-D-Glucoside, and supernatant was clarified by 0.8/0.2 μm filtration. The p14endo15 FAST proteins were purified from the supernatant using fast protein liquid chromatography (FPLC) on the AKTA affinity purification system (Cytiva). FAST containing fractions are dialyzed and then undergo cationic exchange purification on the AKTA system. Protein samples were quality control analyzed by SDS-PAGE, Coomassie blue and Western blot; functional validation was done via syncytia formation assay.

### Western Blot

Cells were lysed in ice-cold Pierce RIPA buffer (Thermo Scientific, Cat. No. 89900). Protein amount was determined using Pierce BCA protein assay (Thermo Scientific, Cat. No. 23225). Equal amounts of total protein from each lysate were loaded onto Mini-PROTEAN 4–20% Gradient TGX precast gels (BIO-RAD, Cat. No. 456-1095). Separated protein was transferred to nitrocellulose membranes (BIO-RAD, Cat. No. 1620112). Membranes were blocked with fluorescent western blocking buffer (Rockland, Cat. No. MB-070) for 1 hour at room temperature. Primary antibodies were diluted 1:1000 in blocking buffer and added to the membranes overnight at 4°C with shaking. Goat anti-rabbit Alexa Fluor 680 (Thermo Scientific, Cat. No. A27042), donkey anti-goat Alexa Fluor 680 (Thermo Scientific, Cat. No. A-21084), or goat anti-mouse Alexa Fluor 750 (Thermo Scientific, Cat. No. A-21084) were diluted 1:10000 in blocking buffer and added for 1 hour at room temperature in the dark. Membranes were visualized on the LI-COR Odyssey.

### Syncytia Formation and Inhibition

QM5 quail fibrosarcoma cells were seeded at a density of  $3.5 \times 10^5$  in twelve well cluster plates in Medium 199 containing 10% FBS and cultured overnight before transfecting with Lipofectamine 2000 and 1 μg of pcDNA3 plasmid expressing either p14, p14endo15, or p15 per manufacturer's instructions. Cells were fixed in 3.7% formaldehyde in HBSS at the indicated intervals post-transfection and stained with Hoechst 33342 and WGA-Alexa 647 per manufacturer's instructions. Images ( $n=5$ ) of each condition were captured on a Zeiss Axio Observer A1 inverted microscope at predetermined coordinates within the well ( $n=3$ ). Syncytia were then manually identified with syncytial and total nuclei quantified using FIJI imaging software.

### Lipid Formulations

The lipid formulations designated as 28M, 33T, 37N and 41N were made by combining the cationic lipid (DOTAP), ionizable lipid (DODAP), helper lipid (DOPE) and PEGylated lipid (DMG-PEG2000) in the following lipid molar ratios: 28M (24:42:30:4), 33T (42:24:30:4), 37N (6:60:30:4) and 41N (0:66:30:4). The lipids were heated in a 37°C water bath for 1 min, vortexed for 10 seconds each, then combined and vortexed for 10 seconds. The combined lipid mixture was dehydrated in a rotavapor at 60 rpm for 2 hours, under vacuum, then rehydrated with 14 mL 100% ethanol, and sonicated (Branson 2510 Sonicator) at 37°C, set to sonication of 60. The lipid formulation was aliquoted in 500 μL batches and stored at -20°C. MC3-LNP formulation was composed of DLin-MC3-DMA/DSPC/Cholesterol/DMG-PEG2000 with the molar ratio 50:10:38.5:1.5.<sup>11</sup> ALC-0315 LNP formulation was composed of ALC-0315/DSPC/Cholesterol/ALC-0159 (PEG-Lipid) with the molar ratio 46.3:42.7:1.6:9.4. SM-102 LNP formulation was composed of SM-102/DSPC/Cholesterol/DMG-PEG200 at a molar ratio of 50:38.5:1.5:10.<sup>102</sup> The physical characteristics of these lipids have been reviewed elsewhere.<sup>103</sup>

### Nucleic Acid Quantification

Nucleic acid concentration and purity was measured via absorbance at 260 nm and 280 nm using the Nanodrop method according to the manufacturer's instructions (Nanodrop 2000 Spectrophotometer, Thermo Scientific, Edmonton, Canada).

### FAST-PLV Construction

The FAST-PLVs were made with lipid formulation 41N unless otherwise stated. The NanoAssemblr Benchtop microfluidics mixing instrument (Precision NanoSystems, Vancouver, BC, NIT0013, and NA-1.5-88, respectively) was used to mix the organic and aqueous solutions and make the PLVs. The organic solution consisted of lipid formulation. The aqueous solution consisted of nucleic acid cargo, 5 nM FAST (p14endo15) protein, and 10 mM acetate buffer (pH 4.0). The Benchtop NanoAssemblr running protocol consisted of a total flow rate of 12 mL/min and a 3:1 aqueous to organic flow rate ratio. PLVs were dialyzed in 8000 MWCO dialysis tubing (BioDesign, D102) clipped at one end. The loaded tubing was rinsed with 5 mL of double distilled water and dialyzed in 500 mL of Dialysis Buffer (ENT1844) with gentle stirring (60 rpm) at ambient temperature for 1 hour and was repeated twice with fresh Dialysis Buffer. PLVs were concentrated using a 100 kDa Ultra filter (Amicon, UFC810096) according to the manufacturer's instructions. PLVs were filter sterilized through 0.2 µm Acrodisc Supor filters (Amicon, UFC910008).

### In Vitro Transfection

Cells were counted using a hemocytometer, and 3,000-5,000 cells were seeded to 96-well or 20,000-40,000 cells to 48-well tissue-culture treated plates and left overnight. The cells were transfected with 10-2000 ng of pDNA encapsulated in FAST-PLVs, MC3-LNPs, or Lipofectamine 2000 for 96-well plate (300µL cell culture media final) and 1000 ng for 48-well plates (1000µL cell culture media final). Lipofectamine 2000 was prepared according to manufacture instructions. The optimal transfection time for mRNA is 24-48 hours and 72-96 hours for pDNA. A luciferase reporter assay was used to measure expression levels of FLuc in different cell lines. Cell culture media was removed from cells growing in a 96-well plate, and cells washed with 1x PBS. A 50-microliter aliquot of reporter lysis buffer (Promega E397A) was added to the cells. The cells were mixed and incubated at room temperature for 10-20 mins. D-luciferin (150µg/mL, GOLDBIO, LUCK-100) was dissolved in 100mM Tris-HCl (pH 7.8), 5mM MgCl<sub>2</sub>, 2mM EDTA, 4mM DTT, 250µM acetyl-CoA, and 150µM ATP.<sup>104</sup> The luciferin substrate (100 µL) of was added to each well immediately before measurement. Luminescence was measured via the FLUOSTAR Omega fluorometer using the MARS data analysis software for analysis. Green fluorescent protein (GFP) or mCherry expressing cells were processed for flow cytometry analysis. The cells were trypsinized and resuspended in 400 µL (per well of 48 well plate) of FACS buffer, then transferred to a 5 mL flow cytometry tube (SARSTEDT 75X 12 mm PS Cat. no. 55.1579) and analyzed with a BD LSRII Fortessa X20 SORP. Mean fluorescence intensity (MFI) presented on the Fluorophore<sup>+</sup> population unless otherwise stated. cGAMP ELISA conducted 24 hours after transfection using DetectX 2'3' – Cyclic GAMP Enzyme Immunoassay Kit (Arbor Assays, Ann Arbor, USA) following manufacture specifications.

### Confocal Microscopy

ARPE-1 cells are labeled with CellLight™ Early Endosomes-GFP BacMam (Cat. No. C10586, Thermo Scientific, Edmonton, Canada), which expresses a fusion construct of Rab5a and GFP. 48 hours later, siRNA targeting HPRT1 conjugated to Cy5 is encapsulated within FAST-PLVs or MC3-LNPs and added to transduced ARPE-1 cells at a concentration of 10µg/mL. 1 hour later cells are extensively washed with PBS and fixed with 3.7% formaldehyde and mounted using ProLong Gold containing DAPI (Cat. No. P36931, Thermo Scientific). Mounted slides are imaged on Nikon Confocal A1R microscope (Nikon Instruments Inc., Melvill, USA) using a 60X objective lens with immersion oil.

### Imaging Flow Cytometry and Endocytosis Inhibition

ARPE-1 are incubated with 125µM Dynasore at 4°C for 30 minutes, following which, media is replaced with pre-warmed media containing 125µM Dynasore and cells are placed in a 37°C incubator for 30 minutes before test articles are added. Control cells are treated with DMSO at 37°C. Alexa Fluor 488 labeled EGF (Cat. No. E13345, Thermo Scientific) is added to Dynasore and DMSO treated cells for 30 minutes at 37°C before cells are extensively washed and prepared for imaging flow cytometry. siRNA targeting HPRT1 conjugated to Cy5 is encapsulated within PLVs formulated with and without FAST protein. 10µg/mL is added to Dynasore and DMSO treated cells for 1 hour at 37°C before cells are extensively washed and prepared for imaging flow cytometry. During the last 10 minutes of treatment, CellMask Deep Red (Cat. No. C10046, Thermo Scientific) or CellMask Green (Cat. No. C37608, Thermo Scientific) and Hoechst 33342 (Cat. No. H21492, Thermo Scientific) was added to the cells. Cells are resuspended in 40µL FACS buffer and analyzed on Amnis ImageStream X MkII (EMD Millipore, Seattle, USA) with at least 10,000 events captured. IDEAS 6.2 software was utilized to analyze images. Doublets are first removed, and only focused cells analyzed. To assess EGF-AF488 uptake, the guided analysis wizard for internalization was used.<sup>105</sup> To assess siRNA-Cy5 uptake, first an analysis mask encompassing the interior of the cell that omits the CellMask plasma membrane stain was generated. Cy5 mean fluorescence intensity was then calculated on this internal area (Internalized Cy5 Intensity).

### PLVs Characteristics and Encapsulation Efficiency

PLVs made by NanoAssemblr Benchtop were diluted 1:50 to 1:20,000, depending on concentration, with twice 0.2 µm syringe-filtered PBS buffer. Particle size, polydispersity index (PDI), and zeta potential was measured on final samples using the Malvern Zetasizer Range and a Universal 'Dip' Cell Kit (Malvern, ZEN1002) following the manufacturer's instructions. The nucleic acid encapsulation efficiency was calculated using a modified Quant-it PicoGreen dsDNA or Quant-it RiboGreen RNA assay with the following modifications to the assay protocol (Thermo Scientific, Edmonton, Canada). PLVs were mixed 1:1 with TE + Triton (2%) to obtain the Total DNA Concentration, or with TE alone to obtain the Unencapsulated DNA Concentration. The DNA standards were also diluted in

TE + Triton (2%), and samples were and incubated at 37°C for 10 min, then diluted a final time with TE + Triton (1%) or TE alone, plated in a black 96 well flat-bottomed plate, and measured with a FLUOstar Omega plate reader (BMG Labtech, 415-1147). Encapsulation efficiency was calculated by using the following equation:

$$\text{Encapsulation Efficiency} = \frac{\text{Total DNA Concentration} - \text{Unencapsulated DNA Concentration}}{\text{Total DNA Concentration}} \times 100$$

### Atomic Force Microscopy

Final FAST-PLVs encapsulating pDNA were evaluated by Atomic Force Microscopy (AFM, Bruker Dimension Edge) for visual validation of the measured particle size. The PLVs were diluted with 0.1 μm filtered PBS to 0.1 μg/mL. An aliquot (2 μL) of the diluted sample solutions was immediately spread on a clean glass slide. The sample was dried at ambient temperature (25°C) for 5 min and any excess aqueous solution was removed with filter paper. The sample was dried for another 15 minutes before imaging at a scan speed of 1 Hz. Tapping mode was carried out using a Ted Pella Tap300 cantilever with a quoted spring constant of 20–75 N/m. 2 D and 3 D images of different zones were examined due to the limitation of small, scanned areas by AFM. Height, Phase and Amplitude mode was used for image analysis using Gwyddion software.

### Transmission Electron Microscopy

Final FAST-PLVs encapsulating pDNA were evaluated by transmission electron microscopy. 5μL aliquots of thousand-fold diluted FAST-PLVs, were placed on 300 mesh carbon-coated copper grids for an hour to dry on the surface, followed by two washes with 0.1μm filtered water. After removal of excess liquid, samples were negatively stained using 0.1μm filtered 1% uranyl acetate. The dried samples were examined in a JEOL JEM-ARM200CF S/TEM electron microscope.

### Viability Assay with Alamar Blue

Cell cultures in a 96 well plates were treated with test compounds at indicated concentrations. For lipid toxicity, purified lipids were dissolved in ethanol and a dilution series was generated. 1μl of each lipid stock was added to 200μl of cell culture media. After 24–96 hours, a 1/10 volume of Alamar blue solution (440 μM Resazurin; Sigma R7017 5GM) was added to the cells in culture medium and incubated for 2-4 hours at 37°C 5% CO<sub>2</sub>. The Omega Fluostar (BMG LabTech) plate reader was used to measure the fluorescence (excitation wavelength of 540 nm and emission at 590 nm) of the treated cells. Cell viability was calculated using the following formula:

$$\text{Viability} = \frac{\text{Treated Absorbance} - \text{Media Background Absorbance}}{\text{Vehicle Absorbance} - \text{Media Background Absorbance}}$$

### Lactate Dehydrogenase (LDH) Cytotoxicity Assay

VERO cells were seeded into 96 well plates, and the CyQUANT LDH Cytotoxicity Assay was conducted to determine the toxicity of different lipid formulations following manufacturers' instructions. In brief, pDNA-FLuc was encapsulated within each lipid formulation (28M, 33T, 37N, and 41N) and added to cells at a pDNA concentration of 1.5 nM. Twenty-four hours after pDNA addition, 50 μL of cell culture media was collected for LDH absorbance. Absorbance was collected at 490nm and 680nm (background), and the 680nm reading was subtracted from the 490nm value. Cytotoxicity was calculated using the following equation:

$$\% \text{Cytotoxicity} = \frac{\text{Lipid Treated LDH Activity} - \text{Vehicle LDH Activity}}{\text{Maximum LDH Activity} - \text{Vehicle LDH Activity}} \times 100$$

To determine toxicity of increasing concentrations of FAST protein, AC10, H1299, and HEK293T cells were seeded into 48 well plates and transfected with PLVs encapsulating 0.7nM pDNA-GFP. 48 hours after transfection, 50 μL of cell culture media was collected for LDH absorbance. Data are represented as background subtracted LDH absorbance values.

### Whole Body and Ex Vivo Bioluminescence

At indicated time points after the injection of the FAST-PLVs, mice were injected intraperitoneally with 0.25 mL D-luciferin (30 mg/mL in PBS) and allowed to recover for 5 minutes. The mice were then anesthetized in a ventilated anesthesia chamber with 2% isoflurane in oxygen and imaged ~10 min after D-luciferin injection with an *in vivo* imaging system (In Vivo Xtreme, Bruker, Montreal, Canada or IVIS Spectrum, Perkin Elmer, Waltham, USA). All images are taken with a PBS injected control mouse to serve as a reference point to determine the lower threshold of each image. Quantification of the luminescent signal was done using Bruker Molecular Imaging Software (whole-body images only) or Perkin Elmer Living Image Software. For whole-body images taken on the Bruker In-Vivo Xtreme, a manual ROI was drawn to encompass the entire area of each mouse. The sum intensity (photons/second) from the control mouse was subtracted from the sum intensity from each experimental mouse to normalize different timepoints and control for background signal drift on each image. For ex vivo images taken on the IVIS Spectrum, 30 mg/ml D-Luciferin was mixed at a 1:1 ratio with the *in vitro* 150μg/mL D-Luciferin described above<sup>104</sup> and added to the organs immediately before imaging. Control mouse organs were included with each set as a reference point. A manual ROI was drawn to encompass the entire organ and the average radiance (photons/second/cm<sup>2</sup>/steradian) is reported.

### Biodistribution of pDNA in excised tissues

Adult green monkeys (*Chlorocebus sabaeus*) were intravenously infused with 1 mg/kg pDNA encapsulated within FAST-PLVs and sacrificed two days later. DNA was isolated using the DNeasy Blood & Tissue Kit (Qiagen, Toronto, Canada) protocol following the manufacturer's instructions. Cells were centrifuged for 5 min at 300 x g, the pellet resuspended in 200 µL PBS, and 20 µL proteinase K was added plus 200 µL Buffer AL (without added ethanol). The mixture was vortexed and incubated at 56°C in a Thermomixer (Labnet International, Inc, Edison, NJ) for 10 min. The levels of pDNA in excised tissues were measured using a PCR assay with primers specific to the pDNA backbone. A standard curve was generated using known amounts of pDNA and used to quantify the amount present in each tissue. Data are normalized to the tissue mass for each organ.

### Meso Scale Discovery – Cytokine and Chemokine Quantification

The Meso Scale Discovery QuickPlex SQ 120 (MSD, Rockville, MD) was used with mouse and non-human primate samples as per the manufacturer's instructions. The data was analyzed with MSD Workbench 4.0 software, following the software protocol. The Meso Scale Discovery V-PLEX NHP cytokine 24-Plex Kit (MSD, Rockville, MD) was used to quantitatively determine serum concentrations of 24 proinflammatory cytokines, including IFN-γ, IL-1β, IL-5, IL-6, IL-7, IL-8, IL-10, IL12/IL23 p40 Subunit, IL-15, IL-16, IL17A, CXCL1, GM-CSF, TNF-α, TNF-β, VEGF, IP10, Eotaxin, MCP-1, MCP-4, MDC, MIP-1α, MIP-1β, and TARC. The Meso Scale Discovery V-PLEX Proinflammatory Panel 1 mouse kit was used to quantitatively determine serum concentrations of 10 proinflammatory cytokines: IFN-γ, IL-1β, IL-2, IL-4, IL-5, IL-6, IL-10, IL-12p70, CXCL1 (KC/GRO), and TNF-α.

### Anti-Drug Antibody Titer: Indirect electrochemiluminescence immunoassay (ECLIA) for p14endo15 and FLuc

Recombinant firefly luciferase protein (NBP1-48355, Novus Biologicals, Centennial, USA) or purified p14endo15 protein was coated on the standard binding plate (Meso Scale Discovery; MSD, Rockville, USA) at 1 µg/mL for one hour at ambient temperature with shaking. The plate was washed three times with 0.05% Tween-20 in PBS followed by the addition of Blocker A (blocking buffer, MSD). After 30 min of incubation, the plate was rewashed with PBS-T. Serially diluted p14endo15 antibody and luciferase antibody standards were prepared in Blocker A. Mouse and nonhuman primate serum samples were diluted 1:100 in Blocker A. The antibody standards and diluted mouse serum samples were loaded to plates and incubated for one hour at ambient temperature with shaking. The plate was washed again with PBS-T followed by the addition of 1 µg/mL sulfo-tag anti-rabbit or anti-goat secondary antibody in standards (Meso Scale Discovery; Rockville, USA), and 1 µg/mL sulfo-tag anti-mouse or anti-NHP secondary antibody in mouse and NHP serum samples (Meso Scale Discovery; Rockville, USA). Read buffer (Meso Scale Discovery; Rockville, USA) was added to the plate after washing with PBS-T, and the plate was read in MESO QuickPlex SQ 120 (Meso Scale Discovery; Rockville, USA). The lower limit of quantification (LLOQ) for both assays was 50 ng/mL.

### MicroVue Complement C3a C4d and SC5b-9 Enzyme Immunoassay

The levels of fragments of complement components such as C3a, C4d, and SC5b-9 in NHP serum were measured to determine whether PLVs activated the complement system (C3, C4 and C5). After PLVs were administered, blood was collected at 0.5, 1.0, 1.5, and 12 hours and the sera were immediately extracted. 100 µL of serum was used to determine the levels of C3a, C4d, and SC5b-9 using QUIDEL MicroVue complement C3a/C4d/SC5b-9 Plus EIA kits (Quidel A032 XUS, San Diego, CA) according to manufacturer's instructions, including the high and low controls. A sample of serum taken before PLV administration was used to determine baseline levels of C3a, C4d, and SC5b-9. According to the manufacturer's instructions, the FLUOstar Omega microplate reader was used to measure the optical density of the samples.

### Follistatin ELISA

Serum and media follistatin levels were quantified using human follistatin ELISA kit (PeproTech, Cat. No. 900-K299) with slight modification to adapt it to the MSD system. Capture FST antibody was coated on MSD standard binding plate at 1 µg/ml overnight at room temperature with shaking. The plate was washed three times with 0.05% Tween-20 in PBS followed by the addition of Blocker A. After 1 hour of incubation, the plate was rewashed with PBS-T. Serially diluted Follistatin standard was prepared in Blocker A with 10% mouse serum. Mouse serum samples were prepared in Blocker A at a 1:10 dilution. The serum samples and follistatin standards were incubated overnight at 4°C with shaking. The plate was rewashed with PBS-T and biotinylated follistatin detection antibody was added at a concentration of 1 µg/ml for 2 hours at room temperature with shaking. The plate was washed three times with PBS-T followed by the addition of 1 µg/mL sulfo-tag streptavidin (Meso Scale Discovery; Rockville, USA) for 1 hour at room temperature. The plate was washed with PBS-T three times, then Read buffer was added to the plate then analyzed with the MESO QuickPlex SQ 120 (Meso Scale Discovery; Rockville, USA).

### Human Erythropoietin (EPO) ELISA

Serum EPO levels were quantified using the U-PLEX Human EPO Assay kit developed by Meso Scale Discovery (Cat. No. K151VXK-2), following the manufacturer's instructions. Briefly, plates are coated with biotinylated capture antibody prior to sample and standard administration. Samples and standards are incubated on plate for 1 hour at room temperature, following which detection antibody is added for 1 hour. MSD GOLD Read Buffer B (Meso Scale Discovery; Rockville, USA) was added to the plate and then it was analyzed with the MESO QuickPlex SQ 120 (Meso Scale Discovery; Rockville, USA).

### Histology: Immunofluorescence, In-situ hybridization, and H&E staining

Major organs, including the liver, spleen, lungs, and kidneys, were collected, formalin-fixed, and paraffin-embedded 4-6  $\mu\text{m}$  sections were generated. Sections were dewaxed in xylene and rehydrated using graded ethanol to water washes. Samples for H&E staining were stained in hematoxylin for 8 minutes, briefly differentiated in acid alcohol, and blued with Scott's Tap Water (pH 8). Slides were then stained in acidified eosin for 30 seconds, and dehydrated, cleared, and then mounted. Whole slide images were generated using Panoramic SCAN (3D Histech, Budapest, Hungary) and reviewed by a certified DVM pathologist (Greenfield Pathology Services, Greenfield, USA) to evaluate the organ-specific toxicity. Heat-induced antigen retrieval for IF samples was conducted by immersing rehydrated slides in 10mM sodium citrate (pH 6) and heating until boiling occurred. Slides were blocked in 10% normal goat serum (Cat. No. 869019-M, Sigma, Oakville, Canada) with 1% bovine serum albumin (BSA, Cat. No. A9418, Sigma, Oakville, Canada) in TBS with 0.4% Triton X-100 for one hour at ambient temperature. Anti-GFP antibody was diluted at 1:50 in blocking buffer and incubated on slide overnight. Alexa Fluor 488 conjugated goat anti-chicken secondary antibody (Cat. No. A-11039, Thermo Scientific) was diluted to 1:200 in 1% BSA TBS with 0.4% Triton X-100 and added to slides for 1 hour at ambient temperature. Samples were mounted with ProLong Gold containing DAPI (Thermo Scientific, Cat. No. P36931). In-situ hybridization was conducted using the RNAscope Brown kit with GFP probe following manufactures instructions. Gastrocnemius utilized for determining muscle fiber area were flash-frozen in O.C.T. Compound (Fisher Scientific, Cat. No. 23-730-571) and sectioned using a cryostat. 10  $\mu\text{m}$  sections were warmed to room temperature and fixed with 3.7% formaldehyde for 15 minutes. Cells were washed three times with PBS. Sections were covered with 5  $\mu\text{g}/\text{ml}$  wheat germ agglutinin Alexa Fluor-488 (Thermo Scientific, Cat. No. W11261) for 10 minutes at room temperature. Cells were washed three times with PBS and mounted using ProLong Gold containing DAPI. Sections were visualized using EVOS fl inverted microscope (Advanced Microscopy Group, Bothell, USA) and 7-15 images were taken per section. Cross sectional muscle fiber area was determined using MyoVision software.<sup>106</sup>

### QUANTIFICATION AND STATISTICAL ANALYSIS

A two-tailed Student's *t*-test or a one-way analysis of variance (ANOVA) was performed when comparing two groups or more than two groups, respectively. Statistical analysis was performed using Microsoft Excel and Prism 7.0 (GraphPad). Data are expressed as means  $\pm$  s.d. The difference was considered significant if  $P < 0.05$  (\* $P < 0.05$ , \*\* $P < 0.01$ , \*\*\* $P < 0.001$ , \*\*\*\* $P < 0.0001$  unless otherwise indicated). All the statistical details of experiments can be found in the results and the figure legends.

## Supplemental figures

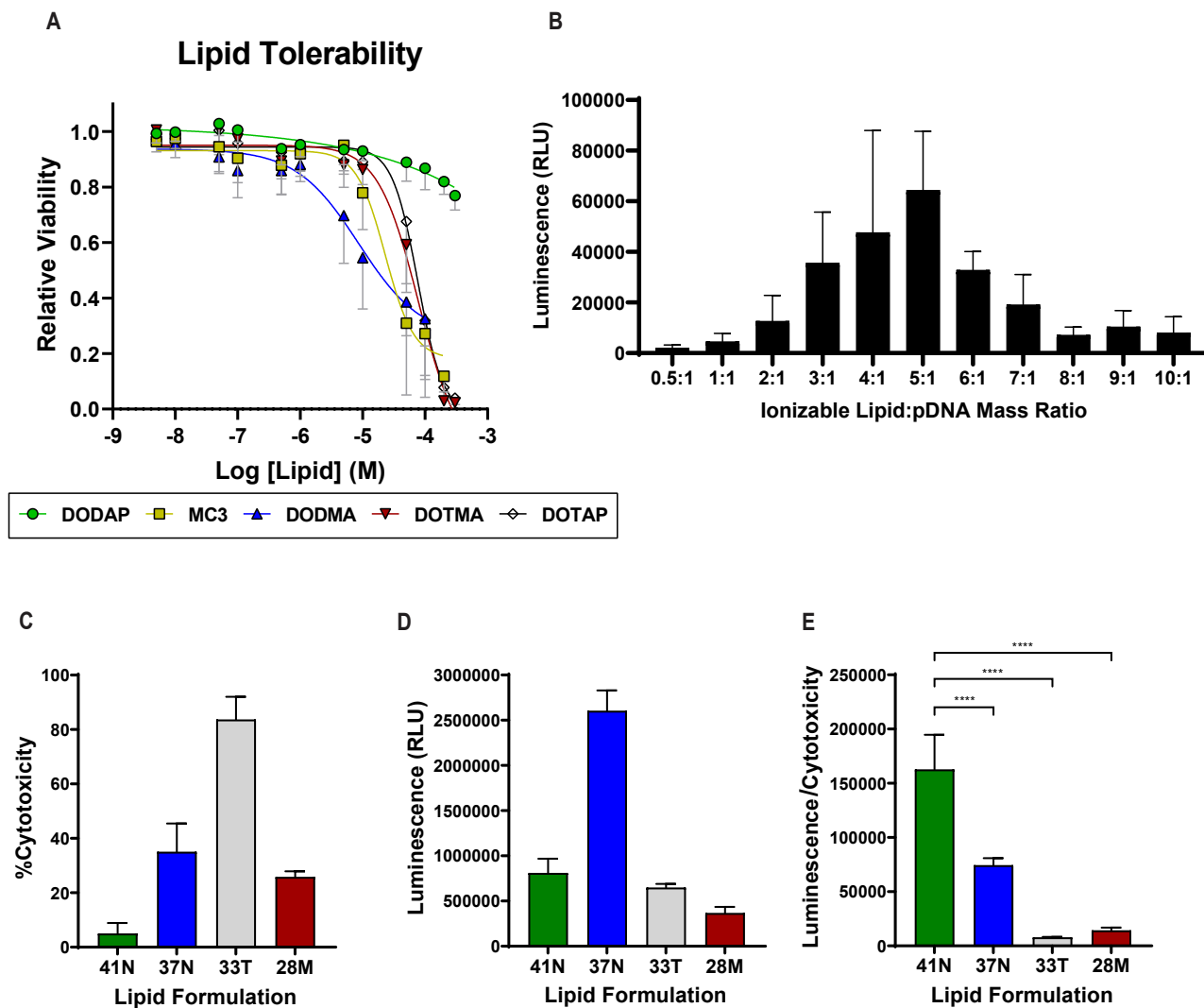
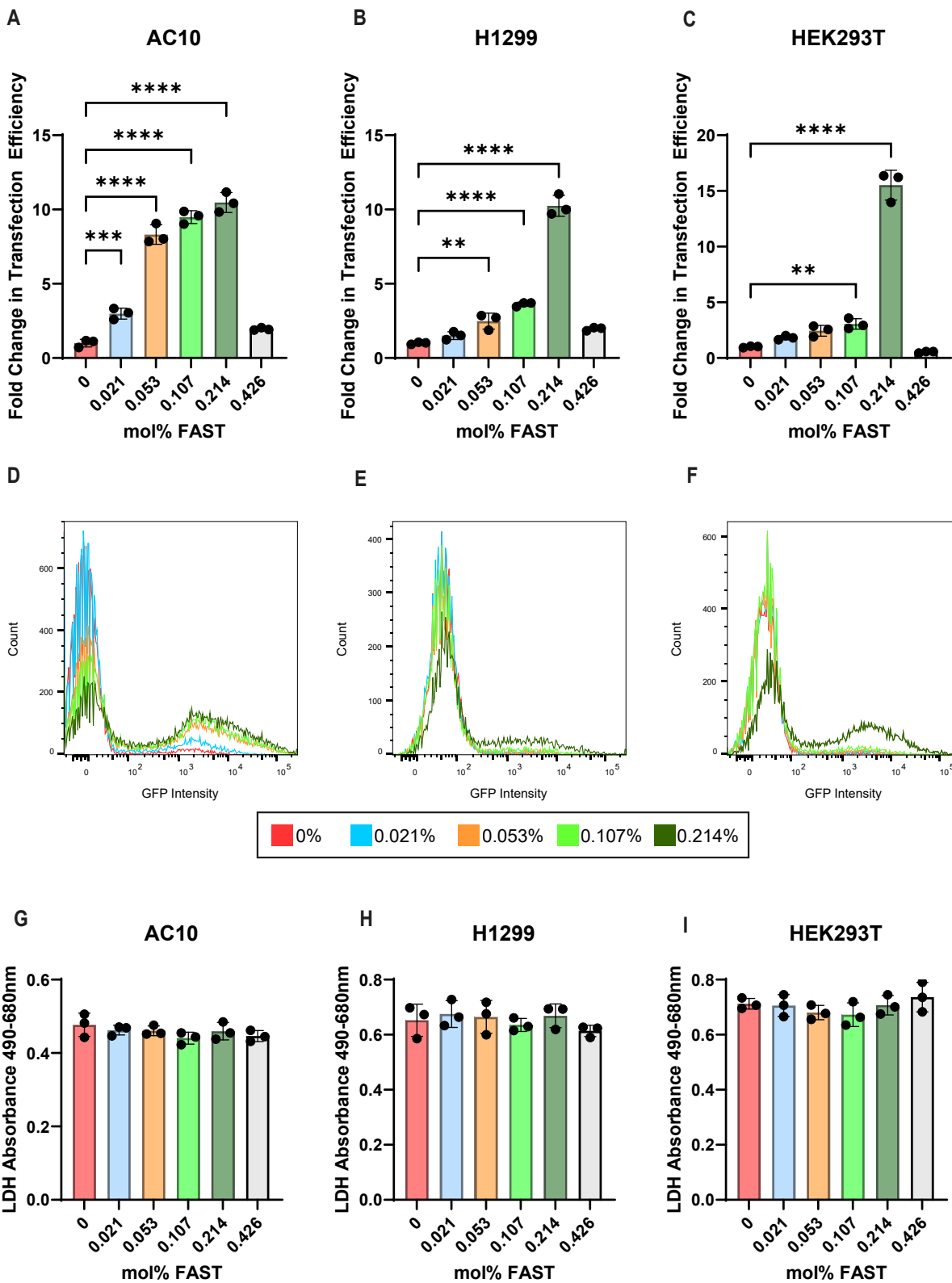


**Figure S1. Optimizing lipid formulation for FAST-PLVs, related to Figure 2**

(A) Tolerability comparison of three ionizable (DODAP, DLin-MC3-DMA, DODMA) and two cationic (DOTMA, DOTAP) lipids determined via Alamar Blue, 72 h after their addition to WI-38 cells.

(B) Effect of different ionizable lipid:pDNA mass ratios on the *in vitro* expression of pDNA-FLuc in ARPE-19 cells 96 h after addition.

(C–E) Comparison of the toxicity and efficacy of four lipid formulations (41N, 37N, 33T, 28M), formulated with FAST protein delivering 1.5 nM pDNA-FLuc to Vero cells. (C) LDH assay used to determine cytotoxicity 24 h after pDNA-FLuc addition. (D) Luminescence determined 72 h after pDNA-FLuc addition. (E) Expression as a function of cytotoxicity. Data are represented as the mean ± standard deviation. One-way ANOVA, Tukey's multiple comparisons, \*\*\* $p < 0.0001$ .



(legend on next page)

---

**Figure S2. FAST protein enhances *in vitro* transfection of pDNA, related to Figure 2**

(A–C) Fold change in transfection efficiency of (A) AC10, (B) H1299, and (C) HEK293T cells, following incubation with 41N PLVs encapsulating 0.7 nM pDNA-GFP with increasing concentrations of FAST protein. Flow cytometry conducted 48 h after transfection. Data are represented as mean  $\pm$  standard deviation,  $n = 3$ . One-way ANOVA, Dunnett's multiple comparisons,  $^{**}p < 0.01$ ,  $^{***}p < 0.001$ ,  $^{****}p < 0.0001$ .

(D–F) Representative GFP intensity histograms from (D) AC10, (E) H1299, and (F) HEK293T cells.

(G–I) LDH absorbance in media of (G) AC10, (H) H1299, and (I) HEK293T cells 48 h after transfection with 41N PLVs encapsulating 0.7 nM pDNA-GFP FAST-PLVs with increasing concentrations of FAST protein. Data represented as mean  $\pm$  standard deviation,  $n = 3$ . One-way ANOVA, Dunnett's multiple comparisons.

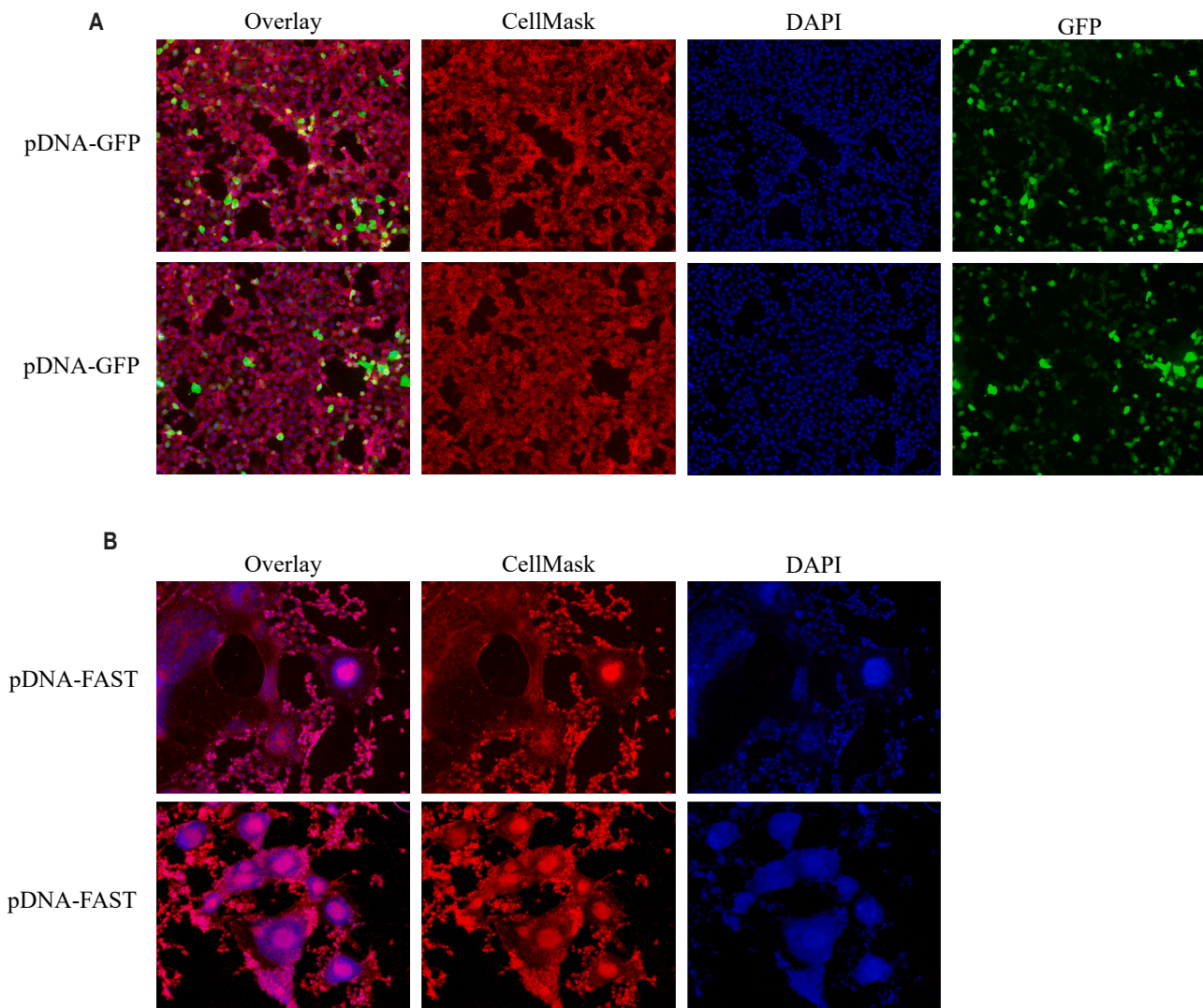


**Figure S3. FAST-PLV transfection does not cause syncytia formation *in vitro*, related to Figure 2**

(A) H1299 cells are incubated with 0.9 nM pDNA-GFP encapsulated within FAST-PLVs; 24 h later cells are stained with DAPI and CellMask-Red and images are collected.

(B) H1299 cells are incubated with 0.9 nM pDNA-FAST encapsulated within FAST-PLVs; 24 h later cells are stained with DAPI and CellMask-Red and images are collected.

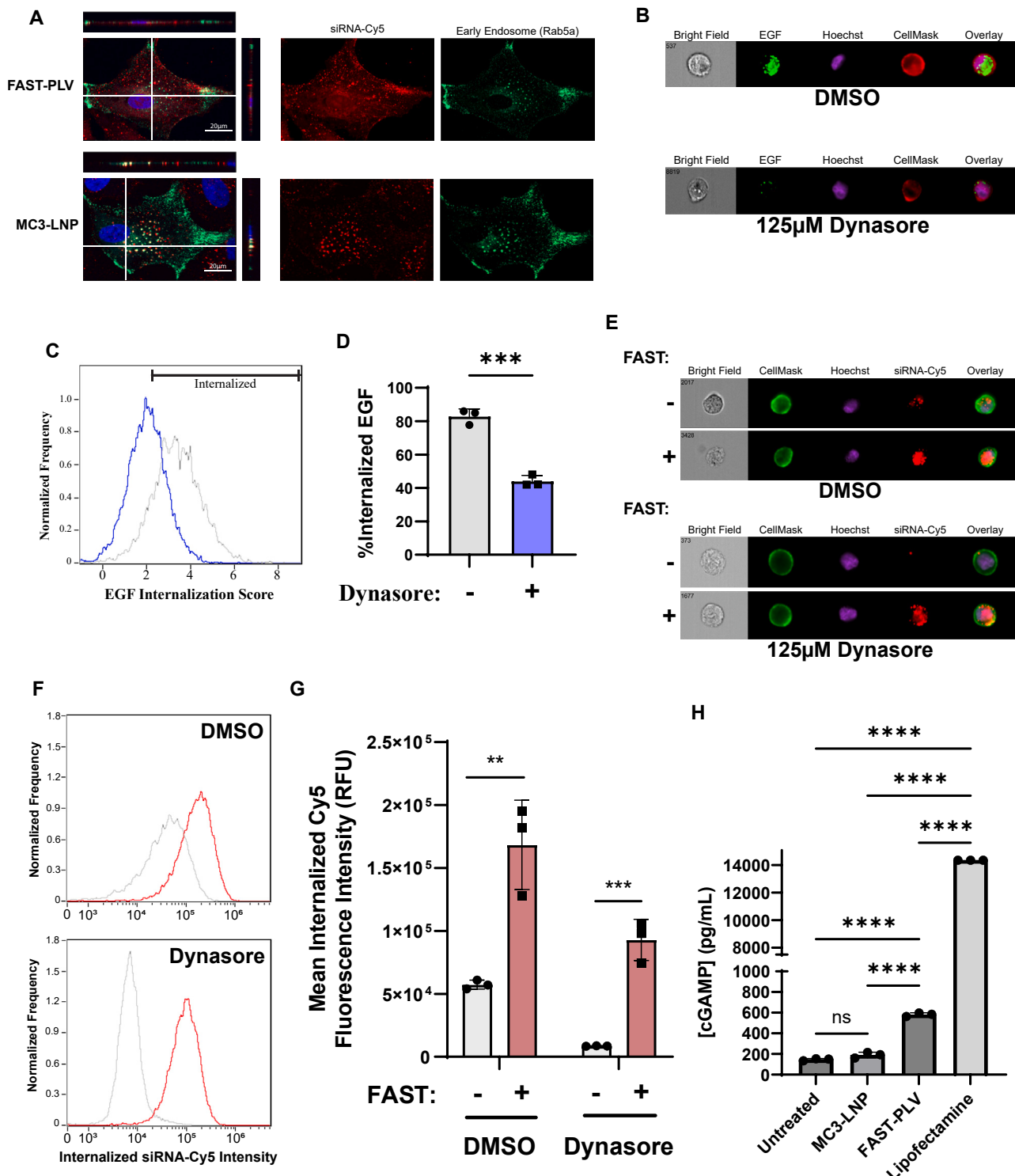


**Figure S4.** FAST-PLV-mediated nucleic acid delivery bypasses endocytosis, related to **Figure 2**

(A) ARPE-1 cells labeled with CellLight Early Endosomes-GFP BacMam are treated with 10 μg/mL siRNA-HPRT-Cy5 encapsulated within FAST-PLVs or MC3-LNPs. Confocal microscopy is conducted to determine endosomal co-localization.

(B) Representative images from imaging flow cytometry that was used to assess the uptake of Alexa Fluor 488-labeled EGF in ARPE-1 cells in the presence and absence of 125 μM dynasore.

(C) Internalization-guided analysis wizard of Image Data Exploration and Analysis Software (IDEAS) used to score internalization of EGF.

(legend continued on next page)

---

(D) Quantification of EGF internalization. Data are represented as the mean  $\pm$  standard deviation, unpaired t test, \*\*\* $p < 0.001$ .

(E) Representative images from imaging flow cytometry that was used to assess the uptake of siRNA-Cy5 encapsulated in PLVs formulated with and without FAST protein in ARPE-1 cells in the presence and absence of 125  $\mu$ M dynasore.

(F) Histogram plots of internalized siRNA-Cy5 intensity in the presence and absence of dynasore. Gray = no FAST protein; red = FAST protein.

(G) Quantification of internalized siRNA-Cy5 intensity. Data are represented as the mean  $\pm$  standard deviation, unpaired t test, \*\* $p < 0.01$ , \*\*\* $p < 0.001$ .

(H) cGAMP ELISA conducted 24 h after transfection of H1299 cells with pDNA-GFP encapsulated within MC3-LNPs, FAST-PLVs, and Lipofectamine 2000. Note, Lipofectamine 2000 resulted in readings above the highest standard, and therefore only the maximum value is reported. Data are represented as the mean  $\pm$  standard deviation. One-way ANOVA, Tukey's multiple comparisons, \*\*\*\* $p < 0.0001$ , ns = not significant.

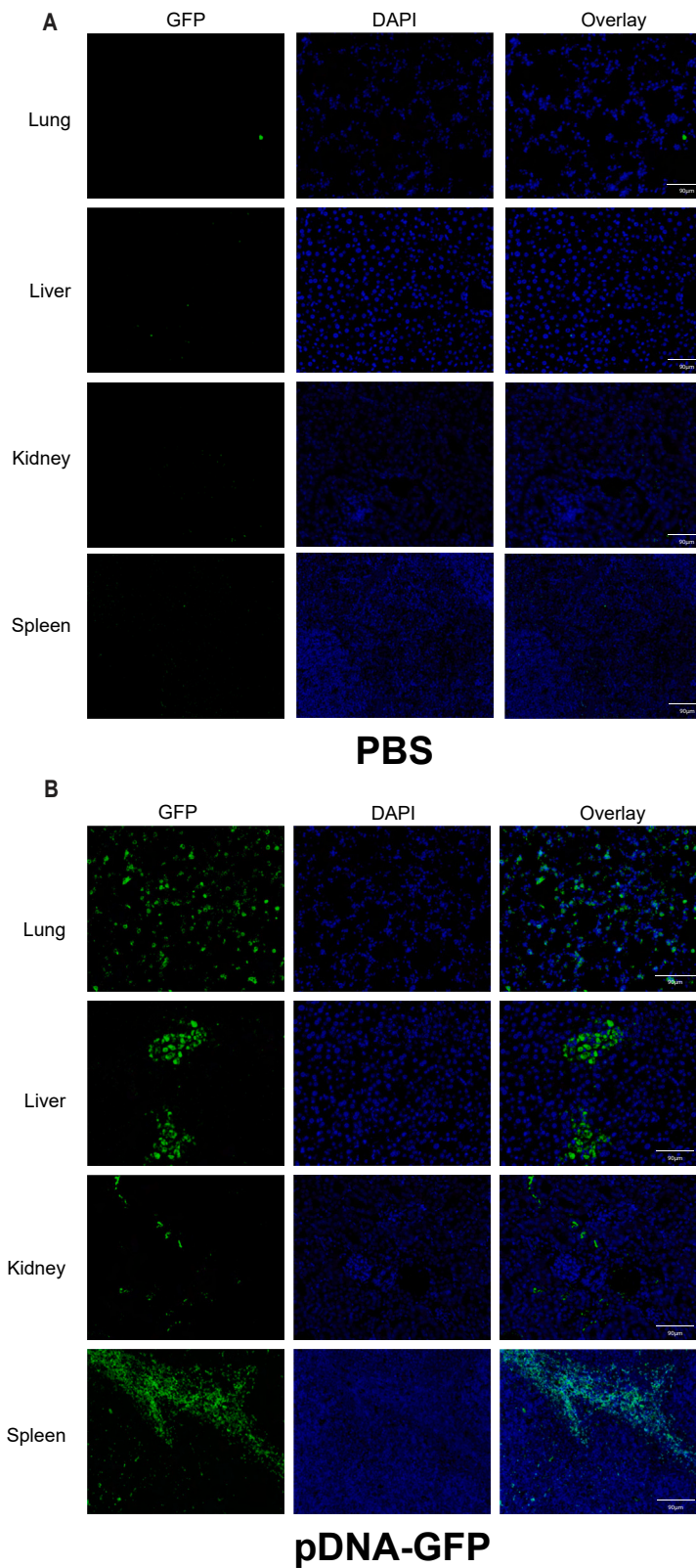


**Figure S5. pDNA-GFP expression in systemically injected mice, related to Figure 3**

(A) GFP immunofluorescence conducted in organs from PBS-injected mice, 24 h after injection.

(B) GFP immunofluorescence conducted in organs from mice injected with FAST-PLVs encapsulating 20 mg/kg pDNA-GFP, 24 h after injection.

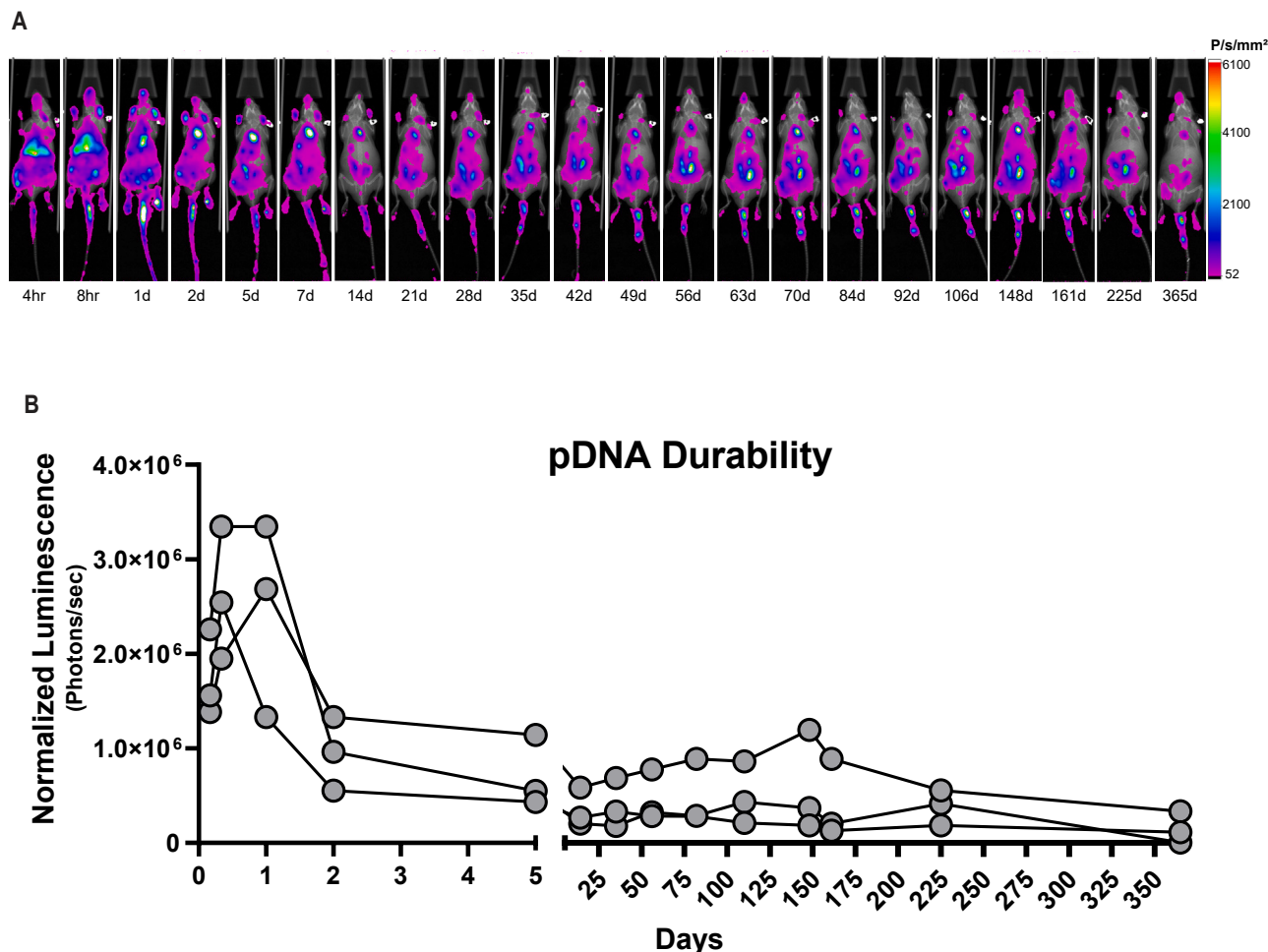
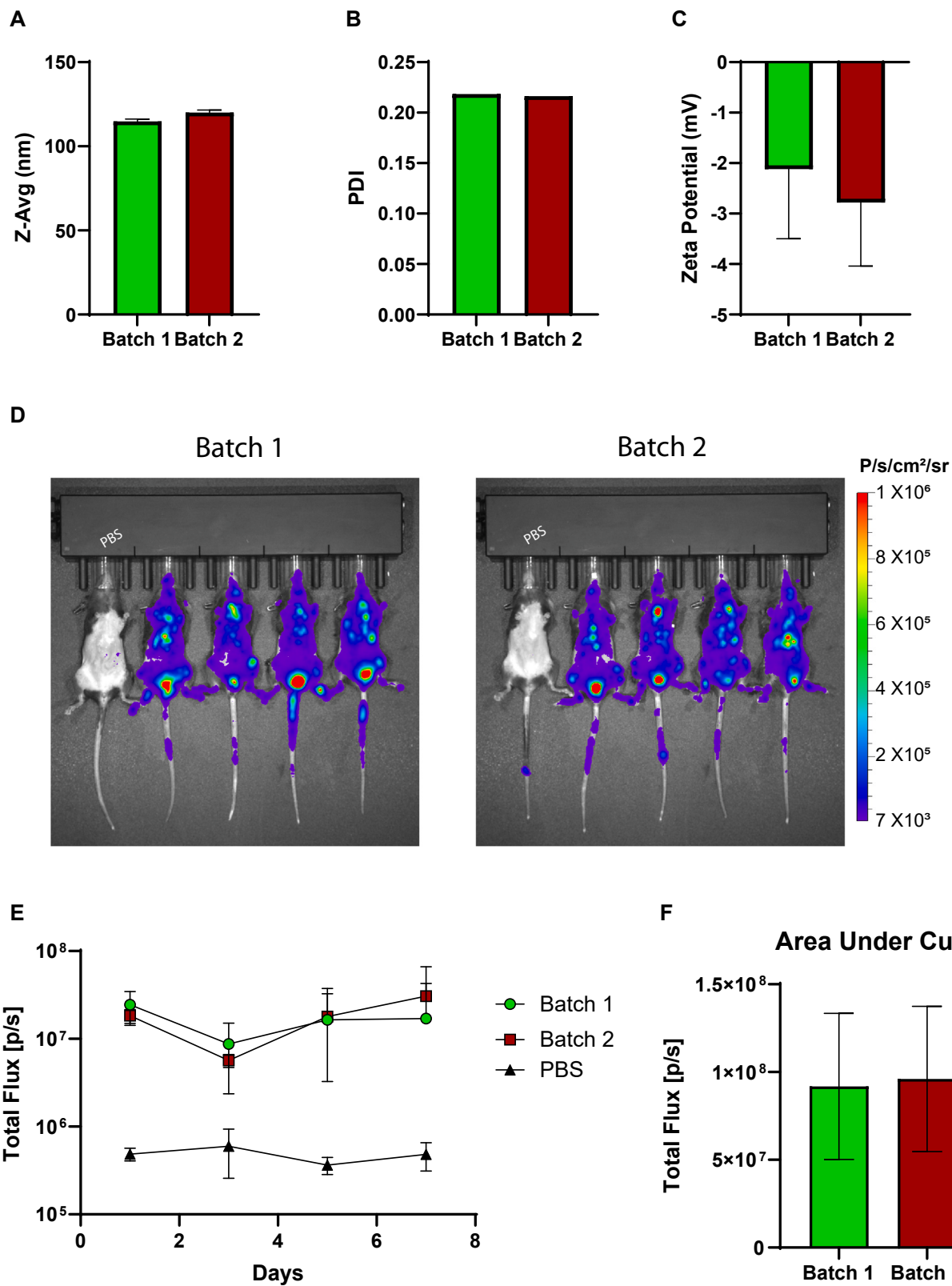


**Figure S6. Durability of pDNA expression in mice, related to Figure 3**

(A) Whole-body bioluminescence of mice injected intravenously with FAST-PLVs encapsulating 20 mg/kg pDNA-FLuc and monitored for 1 year.

(B) Quantification of whole-body bioluminescent signal from mice in (B). Each point from day 7 onward represents a rolling average, where the measurements from 3 weeks were averaged to control for fluctuations in luminescent capture over time.  $n = 3$  biologically independent animals.



(legend on next page)

---

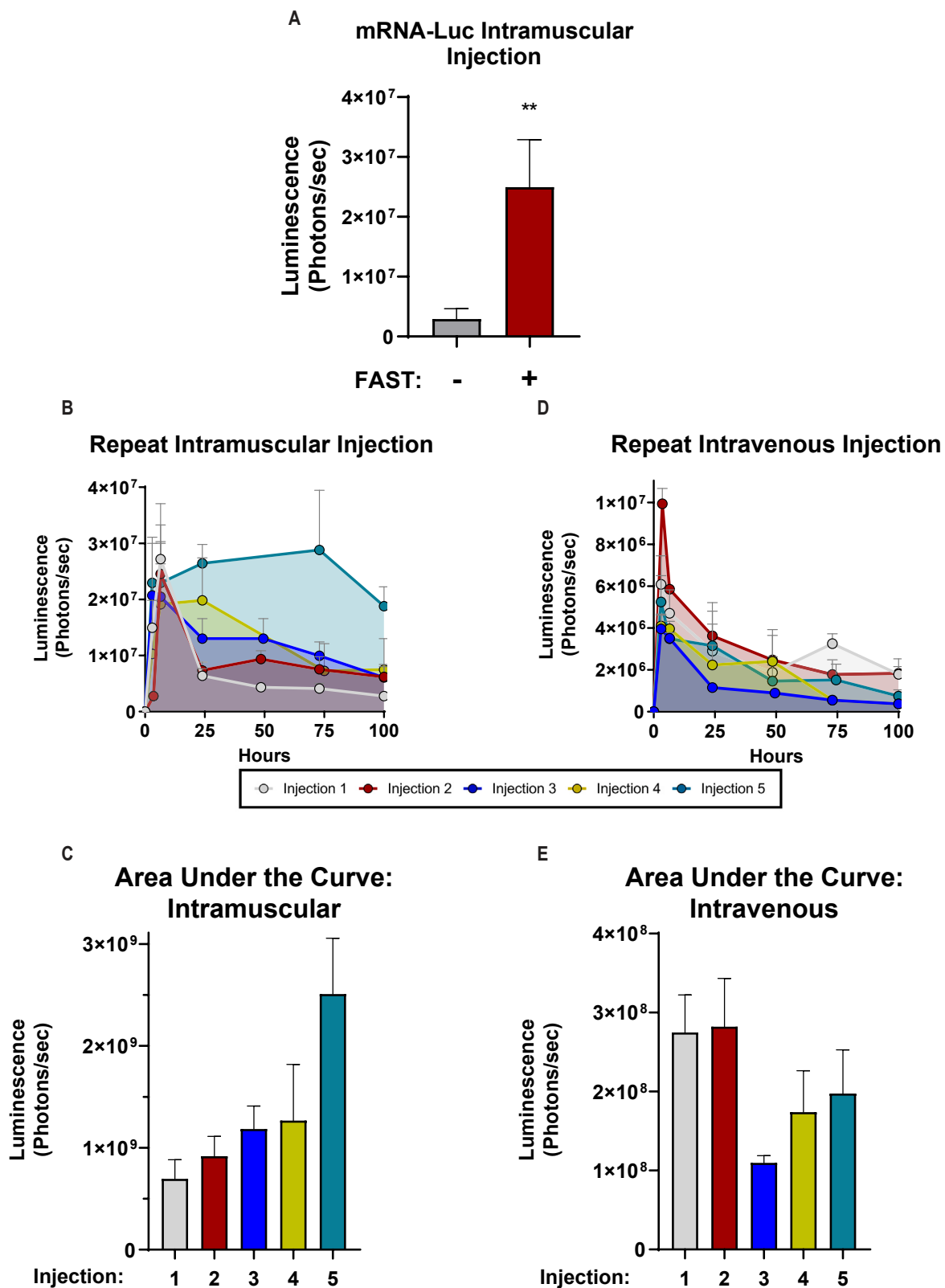
**Figure S7. Comparison of multiple FAST-PLV batches, related to Figure 3**

(A–C) Physical characteristics of two FAST-PLV batches showing (A) Z-Avg, (B) PDI, and (C) zeta potential. Data are represented as mean  $\pm$  standard deviation,  $n = 3$ .

(D) Whole-body bioluminescence of mice injected intravenously with two separate FAST-PLV batches encapsulating 15 mg/kg pDNA-FLuc.

(E) Quantification of whole-body luminescence signal from mice in (A) measured every second day for 1 week. Data are represented as mean  $\pm$  standard deviation,  $n = 4$  biologically independent mice per group.

(F) Area under the curve analysis from the 1-week whole-body luminescence in (B).



(legend on next page)

---

**Figure S8. Delivery of mRNA by FAST-PLVs in mice, related to Figures 4 and 5**

- (A) Quantification of the bioluminescent signal from [Figure 4A](#). Data are represented as mean  $\pm$  standard deviation,  $n = 3$  biologically independent mice per group. Unpaired t test, \*\* $p < 0.01$ .
- (B) Quantification of whole-body bioluminescence from mice in [Figure 5D](#) for 100 h following injection.
- (C) Area under the curve calculated on time course shown in [Figures 5D](#) and [S8B](#).
- (D) Quantification of whole-body bioluminescence from mice in [Figure 5E](#) for 100 h following injection.
- (E) Area under the curve calculated on the time course shown in [Figures 5E](#) and [S8D](#).

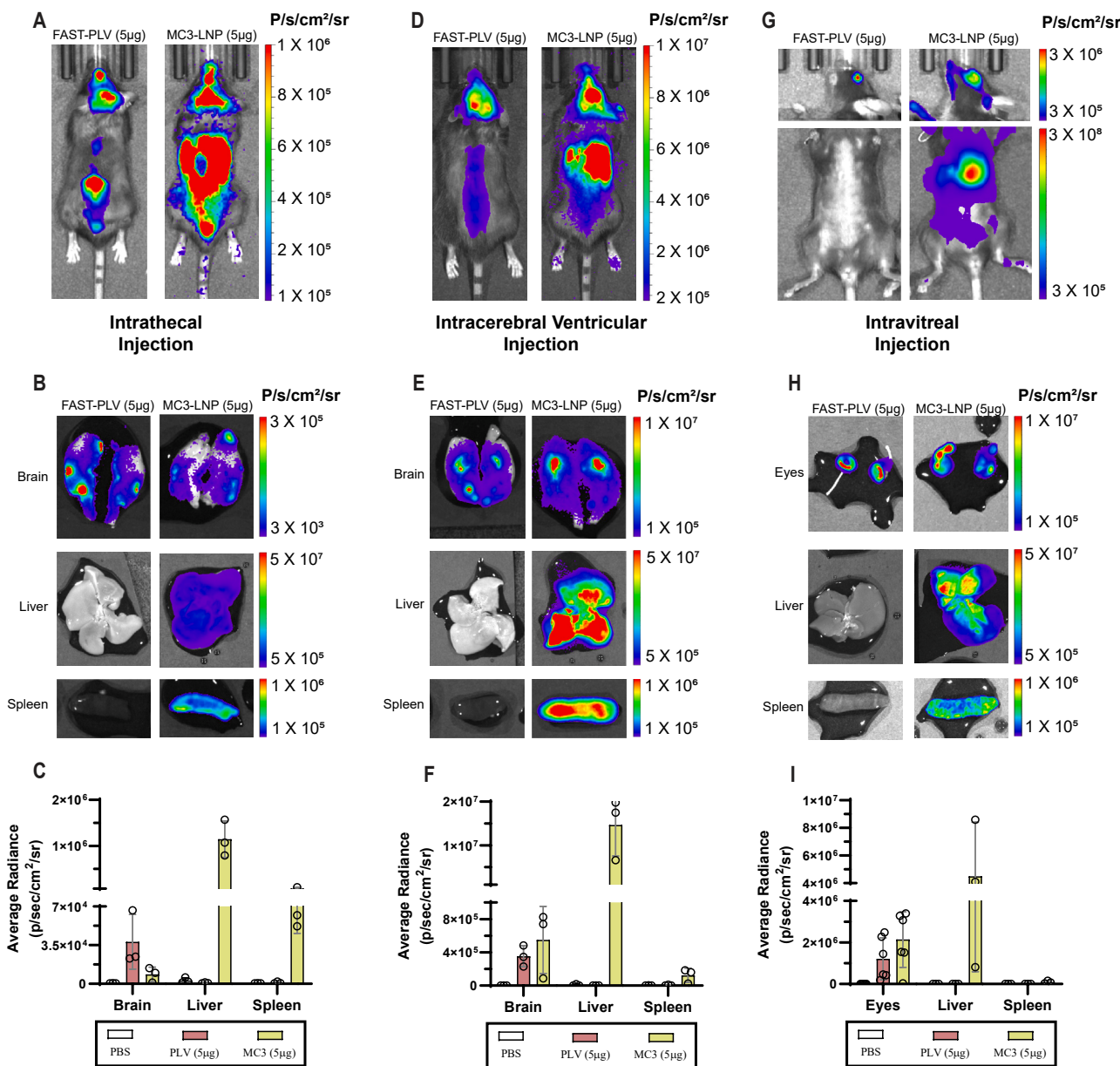


**Figure S9. Comparison of mRNA-FLuc delivery by FAST-PLVs and MC3-LNPs in the CNS and eye, related to Figure 4**

- (A) Whole-body bioluminescent imaging 24 h after intrathecal injection with 5  $\mu$ g mRNA-FLuc encapsulated within FAST-PLVs or MC3-LNPs.
- (B) Ex vivo organ bioluminescent imaging from mice in (A), 24 h after injection.
- (C) Quantification of bioluminescent signal from ex vivo organs presented in (B). Data are represented as mean  $\pm$  standard deviation,  $n = 3$  biologically independent mice per group.
- (D) Whole-body bioluminescent imaging 24 h after intracerebral ventricular injection with 5  $\mu$ g mRNA-FLuc encapsulated within FAST-PLVs or MC3-LNPs.
- (E) Ex vivo organ bioluminescent imaging from mice in (D), 24 h after injection.
- (F) Quantification of bioluminescent signal from ex vivo organs presented in (E). Data are represented as mean  $\pm$  standard deviation,  $n = 3$  biologically independent mice per group.
- (G) Whole-body bioluminescent imaging 24 h after intravitreal injection with 5  $\mu$ g mRNA-FLuc encapsulated within FAST-PLVs or MC3-LNPs into each eye.
- (H) Ex vivo organ bioluminescent imaging from mice in (G), 24 h after injection.
- (I) Quantification of bioluminescent signal from ex vivo organs presented in (H). Data are represented as mean  $\pm$  standard deviation,  $n = 3$  biologically independent mice per group.

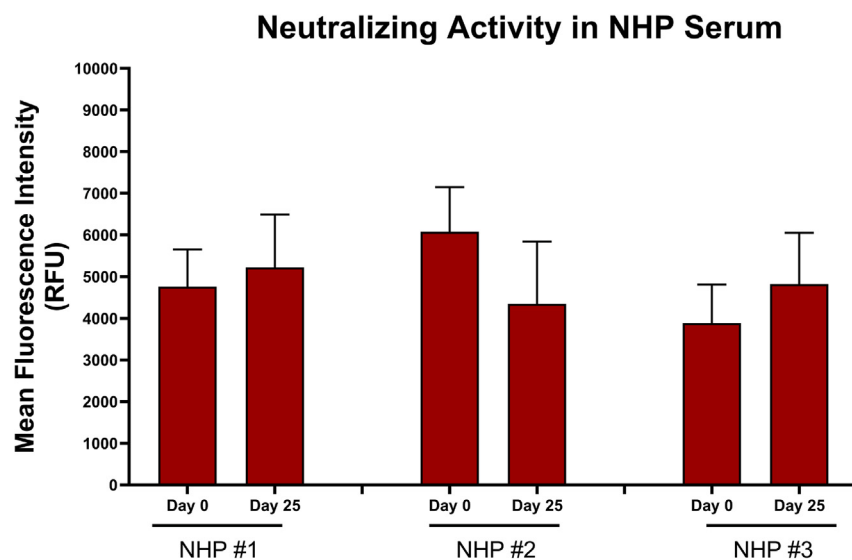
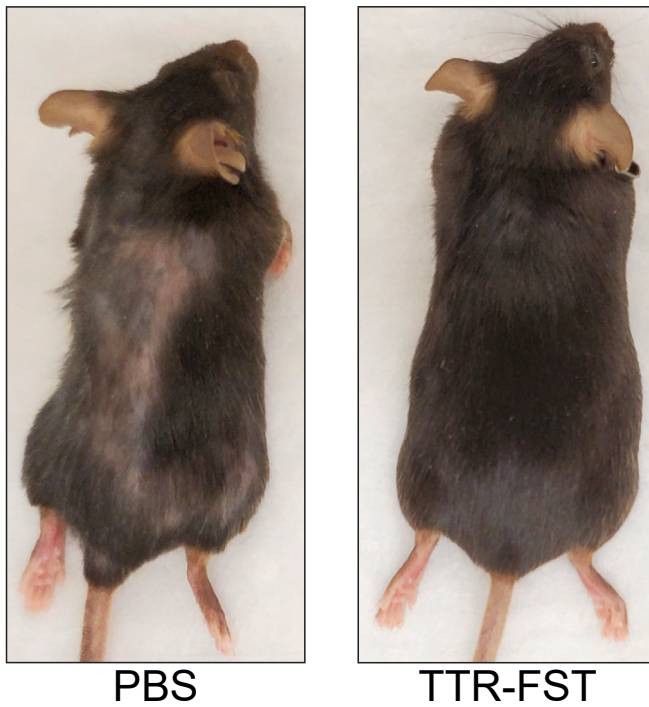


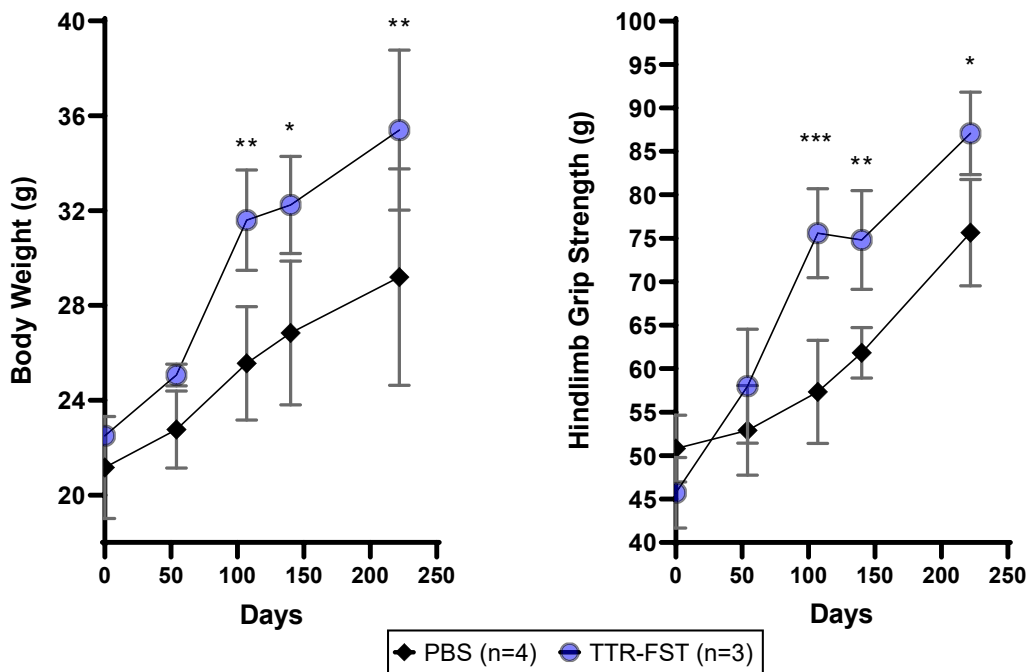
**Figure S10. Immunogenicity of FAST-PLVs in non-human primates, related to Figure 6**

Serum collected from non-human primates prior to FAST-PLV administration and 25 days after administration was incubated with FAST-PLVs encapsulating pDNA-GFP prior to addition to 3T3 cells. Flow cytometry was conducted 96 h after addition, and mean fluorescence intensity of the GFP<sup>+</sup> population is presented.

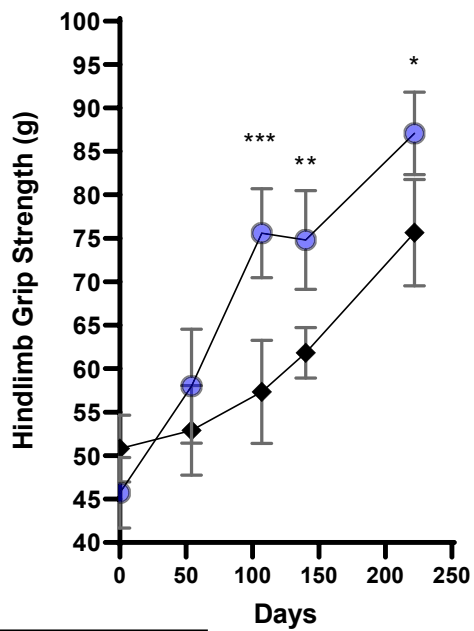
A



B



C



(legend on next page)

---

**Figure S11. Functional improvements following systemic follistatin gene therapy, related to Figure 7**

(A) Representative animals 15 weeks following a single intravenous injection with PBS or FAST-PLVs encapsulating 10 mg/kg pDNA-TTR-FST. Note, hair loss in PBS mouse is likely unrelated to treatment as all cage mates presented with the same condition.

(B) Raw body weight values over several months, following intravenous injection with PBS or FAST-PLVs encapsulating 10 mg/kg of pDNA-TTR-FST. Two-way ANOVA and Dunnett's multiple comparisons, \* $p < 0.05$ , \*\* $p < 0.01$ .

(C) Raw hindlimb grip strength values over several months following intravenous injection with PBS or FAST-PLVs encapsulating 10 mg/kg of pDNA-TTR-FST. Two-way ANOVA and Dunnett's multiple comparisons, \* $p < 0.05$ , \*\* $p < 0.01$ , \*\*\* $p < 0.001$ .